Proposal No. 342
Spokesman: V. Paul Kenney
University of Notre Dame

PROPOSAL TO STUDY NEUTRAL PION PRODUCTION IN 200 GeV/c π^-p INTERACTIONS IN THE 15-FOOT BUBBLE CHAMBER WITH A TRACK-SENSITIVE TARGET

by

R. Louttit and J. Sondericker
Brookhaven National Laboratory

and

N. N. Biswas, N. M. Cason, V. P. Kenney,
W. D. Shephard, and J. M. Bishop
University of Notre Dame

Proposal No. 342
Spokesman: V. Paul Kenney
University of Notre Dame

PROPOSAL TO STUDY NEUTRAL PION PRODUCTION IN 200 GeV/c π^-p INTERACTIONS IN THE 15-FOOT BUBBLE CHAMBER WITH A TRACK-SENSITIVE TARGET

by

R. Louttit and J. Sondericker
Brookhaven National Laboratory

and

N. N. Biswas, N. M. Cason, V. P. Kenney,
W. D. Shephard, and J. M. Bishop
University of Notre Dame

ABSTRACT

We propose to study neutral pion production in 200 GeV/c π^-p interactions in a track-sensitive liquid hydrogen target mounted in the 15-ft bubble chamber with neon/hydrogen filling. We are interested in exclusive channels in which no neutral pions are produced, single-inclusive production of π^0's, two-particle inclusive production and correlations of $\pi^0\pi^0$ and $\pi^0\pi^\pm$ pairs, and cluster-model analyses of events with no missing neutral pions. We request a preliminary engineering run of ~10,000 pictures and a final data run of 200,000 pictures with an average of 4 tracks/picture through the target. The track-sensitive target, with instrumentation and control system, will be supplied by the authors.

1. Introduction

We propose an experiment to study neutral pion production in $\pi^- p$ inclusive, semi-inclusive, and exclusive reactions at 200 GeV/c, using a Track-Sensitive Target (TST) in the 15-ft FNAL bubble chamber. Considerable information now exists on the production of charged particles at Fermilab energies, but data on π^o production is sparse. Data on correlated production of charged and neutral pions is virtually non-existent. Present semi-inclusive studies based only on "charged multiplicity", rather than "total multiplicity" are inconclusive. Event samples in which all secondaries are accounted for (including events in which no π^o's are produced, using the TST in the so-called "veto mode"[1]) will be particularly useful in "clustering" studies. Investigations such as these require the measurement of the charged and neutral pions produced in the same interaction, with $\sim 4\pi$ acceptance, high multiparticle efficiency for charged secondaries and high γ conversion efficiency for π^o decay: requirements met by the 15-ft bubble chamber with a TST.

The physics proposed is complementary to the current study[2] of charged pion production in 205 GeV/c $\pi^- p$ interactions by Notre Dame-Duke-Particle Inst. of Canada, Experiment 2B. Previous studies of inclusive charged[3] and neutral[4] pion production and inclusive strange-particle[5] production in 18.5 GeV/c $\pi^- p$ and $\pi^+ p$ interactions provide a comparison basis for energy-dependence studies and in the case of the π^o production experiment, a means of testing the identification and analysis procedures we will use (with much higher γ conversion efficiency) here.

The Track-Sensitive Target, with its instrumentation and control system, will be supplied by the authors. Brookhaven originated the use of neon/hydrogen mixtures for bubble chambers and has done extensive development and testing of TST designs in the 30-in. and 80-in. chambers[6]. The Notre Dame group has participated in TST development at both Argonne[7] and Brookhaven. The TST configuration proposed here evolved from a series of design studies and tests in the 80-in. chamber by the Brookhaven group, with Notre Dame participation, in 1973-74.

The physics objectives of the experiment are briefly summarized in Section 2. The studies outlined are indicative of the physics to be done with the TST, rather than exhaustive. In Section 3 we consider the general features of TST operation, including radiation length and conversion probability, interactions in the heavy liquid, multiple scattering, phase separation, and target-chamber operating conditions in terms of neon concentration in the chamber liquid. The neon concentration, target length, number of tracks through the chamber and number of pictures (microbarn equivalent) required for the present experiment are established. In Section 4 we discuss the configuration and construction of the target and its mounting, controls, and instrumentation. Measurement procedure and reconstruction software are considered and a schedule of construction, test, and operation is presented.

2. Physics Objectives

a. EVENTS WITH NO NEUTRAL PIONS PRODUCED.

It should be noted that the TST used in the "veto mode" to select a sample of events with no associated γ's is a powerful tool, particularly when used in combination with conventional kinematic analysis to select an "enriched sample" of 4C candidates. We show in Section 3 below that the probability of seeing at least one of the gammas from single π^o production in the present experiment is in the range 94-98%, depending on neon concentration. For events with more than one π^o produced, the chance of discrimination is even higher. Slow neutrons will interact in the heavy liquid.

Events with no neutral particles produced permit a number of interesting analyses, including:

i) Exlusive channels. Diffractive excitation (clustering) of beam and target particle can be studied in the low-multiplicity 4C events. A study by the UC-LBL-FNAL collaboration[8] of 169 events of the type $\pi^- p \rightarrow p\pi^+\pi^-\pi^+$ indicates that the 4 prong - 4C reaction is almost entirely diffractive in character. Definitive diffraction cross sections depend on background subtraction; background in the present experiment should be considerably reduced. A significant contribution from double diffraction is also expected[9].

ii) Inclusive and Semi-Inclusive Analyses. The problem of interpreting inclusive spectra in terms of their semi-inclusive and exclusive constituents can be studied, and the mass "structure" or "clustering" reported in some high energy experiments (see

Diddens, ref. 9) investigated. More generally, clustering behavior of all types can be studied making use of the fact that all final-state particles, regardless of multiplicity, are present in the sample and there are no "missing" neutral particles to wash out or dilute the effects to be expected. Cluster models are discussed in more detail in Section (1d) below.

b. SINGLE INCLUSIVE π^o PRODUCTION

The single-particle inclusive reactions are described in terms of the invariant differential cross section $f(\vec{p}, s) = E\,d\sigma/d^3\vec{p}$ where s is the square of the total c.m. energy and $(\vec{p}, E)$ is the four-momentum of the produced particle. Useful sets of variables are (p_ℓ, p_T^2), (x, p_T^2), and (y, p_T^2) where p_ℓ and p_T are longitudinal and transverse momenta, x is the Feynman variable $p_\ell/p_{max} \tilde{=} 2p_\ell/\sqrt{s}$ in the cms, and the rapidity $y = 1/2 \ln[(E + p_\ell)/(E - p_\ell)]$ can be determined for any frame.

We wish to compare inclusive distributions for π^o production with those for π^- and π^+ production, where the c.m. rapidity distributions $(1/\pi)\,d\sigma/dy$ shown in Fig. 1 are typical. Note that for the produced π^+, Fig. 1b, the 205 GeV/c rapidity distribution is symmetric about $y = 0$ and flat over the central region $y = \pm 1.5$. The distribution for the produced π^-, Fig. 1a, is by contrast asymmetric with respect to $y = 0$, with no indication of plateau development. The difference is not the usual "leading particle effect", which is mani-

fested at much larger y; it will be instructive to see whether the produced π^o behave like the π^+ over the entire rapidity range or show significant differences. When π^o production and $\pi^\pm$ production from 18.5 GeV/c interactions are compared, Fig. 2, it is evident that in the forward hemisphere the π^o distribution is similar to that of the "unlike" charged pion produced from π^+p and π^-p events.

The invariant structure function at $x = 0$ approaches the scaling limit from below, Fig. 3a, while for the target fragmentation region it approaches the limit from above, Fig. 3b. The approach to scaling depends significantly on the charges of the pions in both cases, and additional data for π^o production would be valuable.

c. TWO-PARTICLE INCLUSIVE DISTRIBUTIONS AND CORRELATIONS

Two - particle rapidity distributions $(1/\pi^2)d^2\sigma/dy_1dy_2$ for $\pi^o\pi^o$ and $\pi^o\pi^\pm$ pairs will be compared with those for the charged pion pairs, Fig. 4, where differences in the spectra for the different charge combinations are already evident. Correlation functions

$$C(y_1, y_2) = \rho_2(y_1, y_2) - \rho_1(y_1)\rho_2(y_2)$$

or

$$R(y_1, y_2) = \frac{\rho_2(y_1, y_2)}{\rho_1(y_1)\rho_2(y_2)} - 1$$

where $\rho_1(y) = \sigma_{inel}^{-1} d\sigma/dy$ and $\rho_2(y_1, y_2) = \sigma_{inel}^{-1} d\sigma/dy_1dy_2$ can be measured for $\pi^o\pi^o$ and $\pi^o\pi^\pm$, and compared with data for charged pion pairs. Fig. 5 shows contour plots for the charged pairs, indicating positive short-range correlations in the central region and

suggesting positive correlations for particles with large rapidity separation. Except for the $\pi^+\pi^+$ pairs (where the double peak is not statistically significant), the contours are not symmetric about the diagonal axes, but reach a maximum when both y_1 and y_2 are slightly negative. The difference in behavior of the different charge combinations is already striking; the behavior of the $\pi^o\pi^o$ and $\pi^o\pi^\pm$ combinations is of considerable interest.

A preliminary study of the semi-inclusive correlation functions (in terms of charge multiplicity n, rather than true multiplicity)

$$R^n(y_1, y_2) = \frac{\rho_2(y_1, y_2, n)}{\rho_1(y_1, n)\,\rho_2(y_2, n)} - 1$$

and $$C^n(y_1, y_2) = \rho_2(y_1, y_2, n) - \rho_1(y_1, n)\,\rho_2(y_2, n)$$

for the charged pion pairs is summarized in Table I. The semi-inclusive correlation functions for the central region of rapidity y_1 and y_2 are small, consistent with zero except for the lowest multiplicities. Appreciable differences for the various charge combinations are again evident. The same behavior is evident in 40 GeV/c π^-p interactions studied at Serpukhov[10]. Since the observed inclusive correlations are evidently not reproduced within each order of charge multiplicity, it will be of interest to try further to isolate the dynamical correlation effects in a study of all charge-charge, charge-neutral correlations in terms of total multiplicity[11].

d. CLUSTER EMISSION STUDIES

The question of the grouping of hadrons in separated regions of phase space, and in particular the emission of such groups or "clusters" either multiperipherally or independently, and their subsequent decay, has occupied many authors[12]. "Clustering" is a word that means different things to different people, and can include "fireballs", "resonances" produced diffractively and non-diffractively, or any closer-than-average spacing of particles in rapidity space. In practice, a cluster is defined operationally by the procedure used in the analysis. Thus Berger, Fox, and Krzywicki[13] use a dispersion parameter in rapidity to test whether one has a group of hadrons whose extension in y is small compared to the available range of rapidity. One may therefore distinguish events of the types shown in Fig. 6 (a) and (b). A different analysis technique is suggested by Ludlam and Slansky[14], who define clustering as the existence of two or more components in the final-state amplitude which add incoherently (or nearly so) by virtue of the fact that they occupy distinct population centers in the (3n - 4) - dimensional phase space. They measure the average fluctuation of each event from the overall longitudinal momentum distribution and compare the result with a Monte Carlo reference generated under the assumption that there is no clustering.

Still another type of clustering is envisioned by the production of "clumps" of particles which decay with no final-state interaction of parents or secondaries. Whether or not such clusters are directly

observable in rapidity distributions depends on whether the mobilities of the secondaries are small compared to the spacing of the parent clusters, Fig. 6 (c) or very mobile, Fig. 6 (d). Quigg and Chao[15] have suggested quantum number transfer as a useful parameter in investigating the mobile variety, which are otherwise difficult to identify.

The escape of undetected neutral particles makes the application of any of these analysis techniques, particularly the dispersion test of Berger, Fox, and Krzywicki and the event-to-event fluctuation test of Ludlam and Slansky, rather unrewarding. By contrast the event samples obtained in the experiment proposed, in which the neutral particles are essentially all detected or which contain essentially no neutral particles (Section 1a) will be extremely amenable to cluster analyses. The question of the existence of clustering phenomena, their properties, and their interpretation in terms of particle dynamics may then be pursued.

3. Track-Sensitive Targets: General Considerations

The idea of a track sensitive target (TST) for bubble chambers has been around for some time.[6,7] Literally a bubble chamber within a bubble chamber, the hydrogen-filled TST is surrounded by a neon mixture with short radiation length so that both the charged secondaries from interactions in hydrogen and the conversion electrons from decay of neutral secondaries are photographed for the same event. Some 2.7 million pictures have been successfully obtained by a CERN-Rutherford collaboration with different TST models operated with neon-hydrogen mixtures in the range 73 - 82 molar % neon in the Rutherford 1.5 m chamber.[16]

Some of the more important considerations that go into the general design of a TST for a particular set of experiments are the following:

i) Radiation length vs neon concentration. In the choice of target length there has to be an optimization in terms of event rate in the target and conversion efficiency downstream. Fig. 7 shows radiation length as a function of neon/hydrogen percentage. Table II and Fig. 8 show some of the significant conversion probabilities for a 250 cm nominal conversion path length as a function of neon/hydrogen percentage.

ii) Interaction length vs neon concentration. If the number of interactions downstream from the TST is large, this region will be useless for detecting and measuring gamma conversions. Fig. 7 shows the interaction length for 200 GeV/c π^- interactions for various neon/hydrogen concentrations.

iii) Multiple scattering vs neon concentration. If measurements on charged tracks are continued from the TST to the neon-rich region, the multiple scattering is important. Multiple scattering error $\Delta p/p$ is shown as a function of track length for different (atomic) neon/hydrogen fractions, assuming minimum-ionizing particles in a 20 kG magnetic field, in Fig. 9. Software for matching track segments in the TST and in the chamber has been developed at both RHEL and Berkeley [17].

iv) Phase separation vs neon concentration. A further limitation on the choice of neon/hydrogen concentration is the fact that the neon and hydrogen settle out into two co-existing liquid phases if their temperature drops below a critical temperature shown by the contour [18, 19] of Fig. 10. For operation in the 50 - 80% (mole) concentration region one must remain well above the upper consolute temperature of 29°K. Since the chamber temperature is related to the depth of expansion pressure required to achieve track sensitivity, the operating conditions of the chamber - TST system relate closely to the neon concentration that can be used.

v) Operating conditions vs neon concentration. While the thermodynamic properties of pure hydrogen and neon/hydrogen mixtures which relate to track sensitivity are similar, they are not identical. Bubble density along the track and bubble growth rates in the two liquids will in general be different, depending on the neon concentration. The pressure and/or temperature differences between target hydrogen and chamber liquid required for constant bubble density are shown [20, 6, 7] in Fig. 11. With

a "passive" TST, a cooling loop can be introduced[16] to lower the hydrogen temperature by 1-2° relative to the chamber temperature, maintaining zero pressure difference between TST and chamber.

Discussion. The maximum neon concentration contemplated for the initial 1975 neon/hydrogen running in the 15-ft FNAL chamber is 30 atomic (~45 molar) percent. The Argonne 12-ft chamber was successfully run with ~20 atomic (35 molar) percent in June 1974. We therefore assume for the present proposal that the chamber will be operated with between 20-30 atomic % neon/hydrogen.*

From Fig. 10 it is evident that 20-30 atomic-percent (33 - 45 mole percent) mixtures would require chamber temperatures of ~28 - 28.6° K to prevent phase separation. This is well within the normal temperature range for deuterium operation and presents no problems. Fig. 11 indicates that the hydrogen target should be operated ~0.5 - 1 degree cooler than the surrounding mixture. This is considerably less than the temperature difference maintained in previous TST tests in the Brookhaven 80-in chamber. Fig. 9 indicates that $\Delta p/p$ for multiple scattering on a one-meter minimum-ionizing track will be in the range 2.5 - 3.5% (compared to 1% for pure hydrogen). This will not add significantly to the ~300 μ setting error,

---

* The exact operating condition will be specified after additional experience is obtained with TST running in the Argonne 12-ft chamber (Notre Dame is participating with Exp. E-370 and Brookhaven will be represented by observers) and preliminary running in the 15-ft chamber at Fermilab.

which is determined largely by lens resolution, limited by the depth of field required for the 15-ft chamber.

A number of possible target lengths and configurations have been studied. Considering the requirements of hadron production in the target and conversion of the gammas produced, and also the contribution from hadrons and photons produced in the downstream heavy liquid, we have adopted a target length of 60 inches.* The number of beam tracks per picture must be restricted in order to limit the problem of matching gammas to the proper π^o. An average of 4 tracks per picture through a target with effective length of 130 cm. for hadron production gives an average of 0.5 events per photograph, where $\sigma(\text{TOT}) = 23.96 \pm 0.51$ mb for 200 GeV/c $\pi^- p$ interactions. In the heavy liquid region between the downstream end of the target and a fiducial zone 50 cm from the chamber wall there will, from Fig. 8, be an average of 1.5 additional interactions for the 20 atomic % mixture or 2 additional interactions for the 30 atomic % mixture, for a total of 2 - 2.5 events in each picture. Secondary particle interactions in the neon mixture and events in the target walls will approximately double these figures. If there are ~ 3.5 π^o produced per inelastic event we will average $\sim$ 30-40 gammas total per picture. Many of the gammas originating in the downstream liquid and in the target walls can be eliminated on the scanning table, and the number of gammas produced for an average of 4

---

* We have worked with 57-in TST's in tests in the BNL 80-in chamber. Remaining target dimensions and configuration are discussed in Section 3.

track/picture appears just tolerable for a chamber of this size.

The gamma conversion efficiency depends on the position of the event vertex in the target, the fiducial region allowed for $e^{\pm}$ track identification (and measurement), and the radiation length of the neon mixture used. The LAB angular distribution of π^{o}'s produced in 200 GeV/c $\pi^{-}p$ interactions is assumed to be essentially the same as that of the produced π^{+} mesons, shown in Fig. 12. The distribution consists of a pronounced forward peak, with FWHM $\approx$ 30 m radians, and a broad tail extending to rather large angles.* The half angle subtended from the target center to the downstream end is 33 m radians. For the "Veto mode" study we assume that we will scan for gammas out to a distance of 20 cm from the chamber wall, giving a conversion path in neon/hydrogen $L_c \geq 200$ cm. For inclusive π^{o} production we will require a ~50 cm distance for $e^{\pm}$ track measurement, giving a conversion path $L_c \geq 170$ cm. These are minimum distances in the downstream direction from the outside target dimension. For π^{o}'s produced at large angles or originating at points near the upper and lower faces of the target the conversion path will be larger: $L_c = 250$ cm, for example from a point at the center of the top (or bottom) edge of the TST to a point 50 cm from the chamber wall (as in Fig. 8). Useful conversion efficiencies for these L_c values are compared in Table III assuming 20% and 30% (atomic) neon concentrations. The single gamma conversion effi-

---

* We note that ~52% of the π^{o}'s will be produced with angles that exceed the $\pm 4^{o}$ solid angle acceptance of the gamma-detecting plate in the Exp. 2B hybrid spectrometer used to obtain the π^{+} distribution shown here (Notre Dame data).

ciency for this experiment will be quite high, even for the 20% neon/hydrogen mixture: from 70% for $L_c = 1.7$ m to 83% for $L_c = 2.5$ m. Assuming gammas from multiple π^o production are correctly matched we are interested in the probability of converting at least 1γ from $1\pi^o$, 3γ from $2\pi^o$, 5γ from $3\pi^o$, and 7γ from $4\pi^o$, which for the 20% mixture are respectively 91%, 65%, 42% and 25% for $L_c = 1.7$ m and 97%, 87%, 74%, and 60% for $L_c = 2.5$ m. For the "veto mode" study the limiting condition is $P(\geq 1\gamma[1\pi^o])$, since if more than one π^o is produced the likelihood that at least one γ will be seen is higher. For 20 atomic % neon concentration and $L_c = 2.0$ meter, $P(\geq 1\gamma[1\pi^o])$ is 94%.

The number of pictures required for an exposure, given the other parameters as determined above, depends on the cross sections of the reactions to be studied. The limiting cross section for the present experiment is that of the "4C" events for which no neutral pions are produced ("veto mode" study). The largest contribution to this cross section is the four-prong 4C reaction $\pi^- p \rightarrow p\pi^-\pi^+\pi^-$, for which the cross section is $635 \pm 61 \mu b$[13]. We estimate the total "4C" inclusive cross section at ~3 times this value, or ~2 mb. To obtain a sample of ~2500 events of the 4-prong 4C reaction or ~8000 inclusive 4C events for "veto mode" analysis we will need an exposure of 4 events per microbarn, or 200,000 pictures.

With a total $\pi^- p$ cross section of 23.96 ± 0.51 mb, for a 4 event/μ barn exposure we expect 96,000 events of all types produced in the TST.

We estimate $< n_{\pi^o} >$ incl. $\cong 3.5$, $\sigma(\pi^o, \text{inclusive}) \cong 73.6$ mb, and 294,000 π^o mesons produced in these events. The expected numbers of π^o production events is listed by π^o multiplicity, assumed to be the same as π^+ multiplicity in $\pi^- p$ interactions, in Table IV. Combining these values with the appropriate gamma conversion efficiencies in Table III gives the number of events expected to be available for physics. Of the expected 15,680 $3\pi^o$ events, for example, with 20 atomic % neon and an effective conversion length of 1.70 m (leaving 50 cm for $e^{\pm}$ track measurement), one obtains ~6,540 $3\pi^o$ events if only 5 out of 6 γ are needed for π^o identification, and ~1,800 $3\pi^o$ events for which all 6 γ are seen.

4. Track-Sensitive Target for the FNAL 15-ft Chamber: Design Considerations.

a) TARGET. If the length A of the target is fixed by the considerations of Section 2, the remaining dimensions B, D and t are fixed by the requirement that the TST volume expand by ~1% to obtain track sensitivity, and the elastic properties of the materials used. For plexiglass acrylic, the modulus of elasticity E and maximum allowable stress S_m are respectively 1.32×10^6 and 1100 psi at the operating temperature of ~26°K. Let B be the minimum TST width and D the minimum depth in the direction of the magnetic field. Assuming the condition of a flat plate with uniform loading w, all edges fixed, then if t is the thickness of the face plate, the maximum allowable deflection

$$y = \alpha \frac{w B^4}{E A t^3}$$

and the maximum bending stress

$$S_m = \beta \frac{w B^2}{A t^2}$$

and $$y = \frac{\alpha}{\beta} \frac{B^2 S_m}{E t} .$$

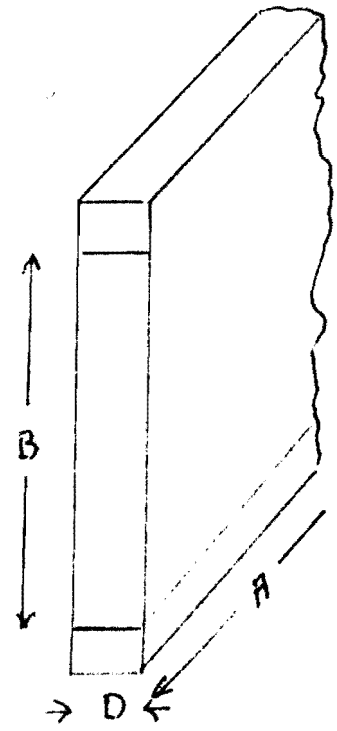

Assuming a total volume displacement $\Delta V/V = 1\%$, then for the approximation indicated,

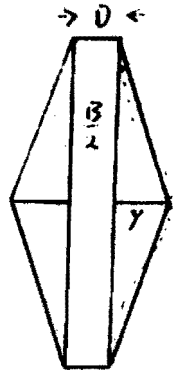

$$\frac{\Delta V}{V} = \frac{\Delta A}{A} = \frac{2\left[2\left(\frac{1}{2}\,\frac{B}{2}\,y\right)\right]}{BD} = .01$$

or $y = .01\,D$

Hence the design limitation

$$.01D \leq \frac{\alpha}{\beta}\,\frac{S_m}{E}\,\frac{B^2}{t} \qquad (6)$$

The length of the target A is 60 in. (64 in. outside dimensions). It would be desirable to limit the outside width dimension so as to clear the 18-in. diameter optics port, so that the target could be mounted and tested without removing the chamber piston. If the width is chosen as 14 in. (17 in. outside dimensions), then from eq. (6), with $\alpha/\beta = .0568$,

$$Dt \leq \frac{(5.68)(1.1 \times 10^3)(1.96 \times 10^2)}{(1.32 \times 10^6)}$$

$$Dt \leq 0.927$$

and for $t = 1/4$ in.

$$D \leq 3.71''$$

It is necessary that D be at least as large as the beam spread, which can be focussed down to ~ a nominal 1 in. A value $D = 2.5$ in. is reasonably conservative from both points of view.

With internal dimensions of 60 in. x 14 in. x 2-1/2 in. the TST will contain a volume of 34 liters of liquid hydrogen. The target will be constructed of acrylic plastic (plexiglass). The side walls will be of 1-1/2 in. type G acrylic, the end walls of

2 in. type G acrylic milled down to 1/2 in. thickness over a 2 in. x 8 in. beam window area. The face sheets will be of 1/4 in. type II UVA acrylic. The target components will be fabricated at Notre Dame and Brookhaven, and assembled at Brookhaven utilizing the instrumentation and auxiliary equipment previously used in the 80-in. chamber TST tests.

The target will be mounted in the 15-ft chamber in a manner similar to that of the CERN-RHEL TST installed in the Argonne 12-ft chamber. Existing lead-throughs will be used for instrumentation and plumbing. For the engineering run, the entire target assembly can be brought in through one of the 18-in diameter optics ports. For physics running it will be necessary to seal off the nose cone volume upstream of the target with a 65-in. diameter disk which will have to be brought up through the piston opening. The overall target configuration is shown in Fig. 13.

b) CONTROLS AND INSTRUMENTATION. The TST proposed will employ the same type controls and instrumentation used successfully with the Brookhaven 80-in. chamber TST test program discussed below. In order to conserve time and manpower Brookhaven will supply the target complete with the previously tested instrumentation, control panel, and electronics. Two D_2 vapor pressure bulbs are used to monitor target temperature, two 4-element strain gauge bridges monitor target pressure (face-plate deflection), a cooling loop

removes up to 60 watts of heat per ^{o}K, and a single vent/fill valve is operated with the control system shown in Fig. 14. Once the chamber is cold, the target is put on automatic servo position control, venting and filling the target as necessary* to keep its plastic windows parallel. This equipment proved extremely reliable in earlier TST tests and removes a large part of the uncertainty from the 15-foot TST program.

c) TST TEST EXPERIENCE AT BROOKHAVEN. Two passive track sensitive targets of the CERN-RHEL type have already been designed, built, and tested in the Brookhaven 80-in. chamber.[21] The first target was successful in reaching track sensitivity with hydrogen both inside and outside the target and ~2,300 photographs were obtained. The addition of the track-sensitive target did not produce any appreciable changes in the thermodynamics of the chamber. Instrumentation and controls as well as the general features of the target design were shown to be satisfactory. Problems were encountered in mixing neon and hydrogen in the chamber, however, and the engineering run was terminated when the procedure adopted to force the breakup of the neon/hydrogen meniscus resulted in the failure of the downstream TST clamp support.

A second TST of the same design was built and tested. A new

---

* A pressure difference $|\Delta p| = 1$ psi between TST and chamber will connect the fill-and-vent valve to the hydrogen reservoir via either the +1 psi bias relay ($p_{target} > p_{chamber}$) or the -1 psia bias relay ($p_{target} < p_{chamber}$), and the TST will fill or vent accordingly.

neon/hydrogen mixing system achieved a uniform liquid concentration within a few hours operation, and an improved support structure (~1300 lb clamping force) proved satisfactory. The neon concentration was ~77 mole %. With the chamber at 29.6° K, the target at 28.7° K, p(chamber) = p(target) = 126 psia, and p_{min} = 75 psia, the chamber, but not the target, was track sensitive, as shown in Fig. 15. During warmup of the TST to its operating temperature a "glue joint" at the bottom edge of the TST failed, terminating the test.

Discussion: Numerous "glue joints" have been designed, built and tested at Brookhaven since the second TST engineering run in a continuing test program of bonding agents and joint design. At present, methods have been developed which increase the cold strength of plexiglass joints by a factor 1.5 x - 2 x the joint strength of the previous 80-in. test targets. The "glue joint" failure in the 80-in. chamber test TST was due to the fact that the face sheet and frame were too highly stressed. The TST configuration proposed for the 15-ft. chamber, Section 4a, is more conservative in design than the test TST in the 80-in. chamber, and in particular the joint stresses are calculated to be considerably smaller. The "glue joint" is therefore no longer of special concern.

Operation of the 15-ft. chamber TST will also be more con-

servative in that the neon concentration will be considerably smaller (30-45 mole % compared to 77 mole % in the 80-in. chamber) and hence the difference in bulk modulus of the target and chamber liquids will be less. An additional factor of improvement has to do with the position of the TST with respect to the travel of the pressure wave front in the chamber. Both the 80-in. chamber and Rutherford targets were mounted vertically so that an appreciable force (1500 lb) was developed across the target during recompression and expansion. Positioning of the TST so that its largest surface is perpendicular to the pressure front reduces the differential pressure to which the target is exposed (500 lb) and therefore further reduces the stress on the structure.

The experience gained in the construction and operation of track sensitive targets at Brookhaven and the reduced stress in the more conservative design provided for the 15-ft. chamber TST will be significant positive factors in providing reliable operation for experiments of the type proposed here.

d) EXPERIMENT SCHEDULE. We are prepared to meet the following schedule to implement TST operation in the 15-ft chamber for the experiment proposed, beginning with the date this proposal is given approval:

i) Approximately 3 months: provide a complete TST with all necessary instrumentation and controls ready for installation in the 15-ft. chamber.

ii) First regular 15-ft. chamber cooldown cycle thereafter: carry out engineering run of ~10,000 pictures to test all components of the TST system in the 15-ft. chamber.

iii) Next regular 15-ft. chamber cooldown cycle: physics run for the experiment proposed.

iv) Within one year thereafter: first physics results.

e) SOFTWARE, MEASURING, AND ANALYSIS. There are several possibilities for track reconstruction and event analysis software. Daniel Bertrand at Brussels has assembled a HYDRA package with TST reconstruction software for their analysis of stopping K^- in their RHEL TST experiment. Jon Guy at RHEL has developed BAGEOM, a modification of HGEOM to analyze the Rutherford TST data. Dennis Hall at LBL has introduced similar modifications into a version of TVGP. We intend to adopt whatever software is standardized for the Argonne 12-ft. chamber TST, provided the experiments there (including Notre Dame's E-370) are run prior to the TST running in the 15-ft. We will use the same scanning and measuring facilities: 5 scanning projectors (4 on-line to a MICRO-810 minicomputer) and 5 measuring projectors on line to a DDP-124 control computer, as we will use to analyze the 12-ft. TST film.

References

1. V. P. Kenney, "Neon-Hydrogen Mixtures and Track-Sensitive Targets for Bubble Chamber Experiments at NAL", SS-24 2610.7, 1969 Aspen Summer Study Vol. II p. 249, National Accelerator Laboratory (1969).

2. W. D. Shephard et al., "One Particle and Two-Particle Distributions and Correlations in 205 GeV/c π^-p Inclusive Reactions", paper presented by V. P. Kenney at the XVII International Conference on High Energy Physics, London (1974).

3. N. N. Biswas et al., Phys. Rev. Lett. 26, 1589 (1971); W. D. Shephard et al., Phys. Rev. Lett. 27, 1164 (1971); W. D. Shephard et al., Phys. Rev. Lett. 28, 703 (1972); J. T. Powers et al., Phys. Rev. D8, 1947 (1973).

4. N. N. Biswas et al., submitted to Phys. Rev. (1974).

5. P. Stuntebeck et al., Phys. Rev. D9, 608 (1974).

6. A. G. Prodell, Rev. Sci. Instr. 36, 1174 (1965); R. C. Albert et al., Advances in Cryogenic Engineering, vol. II, (Plenum Press, New York) p. 321 (1966); R. Huson, "Track Sensitive Targets in the 25-ft. Bubble Chamber", SS-99 2610.7, 1969 Aspen Summer Study vol. II p. 229, National Accelerator Laboratory (1969); J. H. Sondericker, BNL Int. Reports, (1973-74).

7. V. P. Kenney et al., "Design Considerations for the Use of Neon-Hydrogen Mixtures in the 12-ft. Argonne Bubble Chamber", National Laboratory Report ANL-BBC-92 (1967).

8. L. G. Stutte, Ph. D. Thesis, University of California (Berkeley), 1974.

9. P. Schlein et al., Aachen-UCLA-CERN Collaboration, reported by A. N. Diddens, Proceedings of the XVII International Conference on High Energy Physics, London (1974).

10. V. G. Grishin et al., Dubna-Budapest-Bucharest-Warsaw-Krakow-Serpukhov-Sofia-Tbilisi-Ulan-Bator-Hanoi Collaboration, INP Krakow Report 860/PH (1973) and private communication.

11. R. Singer et al., Phys. Lett. 49B, 481 (1974); G. Belletini, Proceedings of the XVI International Conference on High Energy Physics (Batavia), vol. I p. 279 (1972); G. H. Thomas, mini rapporteur talk at XVII International Conference on High Energy Physics, London (1974).

12. C. Quigg and G. H. Thomas, Phys. Rev. D7, 2752 (1973); E. L. Berger and G. C. Fox, Phys. Lett. 47B, 162 (1973); C. J. Hamer, Phys. Rev. D7, 2723 (1973); other relevant papers are referenced by the above authors.

13. E. L. Berger, G. C. Fox, and A. Krzywicki, Phys. Lett. 43B, 132 (1973).

14. T. Ludlam and R. Slansky, Phys. Rev. D8, 1408 (1973); J. Hanlon et al., Phys. Lett. 46B, 415 (1973).

15. A. W. Chao and C. Quigg, Phys. Rev. D7, 2016 (1974).

16. T. F. Coleman et al., Nucl. Instr. & Methods 107, 399 (1973); J. F. Ayres, et al., Nucl. Instr. & Methods 107, 131 (1973); T. G. Coleman et al., Nucl. Instr. & Methods 114, 381 (1974); J. G. V. Guy et al., Proc. Conf. on Instr. in High Energy Physics, Frascati (1973). First physics results with the RHEL TST were presented by B. S. Chaudhary et al. (Bombay), "Dependence of Average π^0 Multiplicity on Charge Topology in $\bar{p}p$ Annihilations at 2 GeV/c" Paper 122, XVII International Conf. on High Energy Physics, London (1974).

17. J. Guy, "BAGEOM: Description of Routines used to reconstruct TST events", RHEL BC Group Physics Note 81, 23.7.74; C.M. Fisher, J.G.V. Guy, and J.W.G. Wignall, Nucl. Instr. & Methods 118, 171 (1974); D. Morrellet, Methods in Subnuclear Physics Vol. 4, part 3, p. 177; G. Gidal (private communication).

18. W.B. Streett and C.H. Jones, Journ, Chem. Phys. 42, 3989 (1965); J.O. Hirschfelder, C.F. Curtis, and R.B. Bird, "Molecular Theory of Gases and Liquids", Wiley, New York (1954).

19. G. Horlitz, S. Wolf, and G. Harigel, Nucl. Instr. & Methods 117, 115 (1974).

20. V.P. Kenney and W.D. Shephard, ND Report 70-26, 8.12.70 (1970).

21. J.H. Sondericker, Particle Detector Div. Technical Notes #18, 20 Brookhaven National Laboratory (1974).

Table I

Values of the Semi-Inclusive Rapidity
Correlation Functions $R(0, 0, n)$ and $C(0, 0, n)$

n	$R^n_{cc}(0, 0)$	$C^n_{cc}(0, 0$	$R^n_{--}(0, 0)$	$C^n_{--}(0, 0)$	$R^n_{++}(0, 0)$	$C^n_{++}(0, 0)$	$R^n_{-+}(0, 0)$	$C^n_{-+}(0, 0)$
4	+0.25 ± 0.23	+0.05	-0.14 ± 0.31	-0.01	-0.42 ± 0.22	-0.02	+0.81 ± 0.43	+0.04
6	-0.07 ± 0.10	-0.06	-0.18 ± 0.15	-0.04	-0.53 ± 0.10	-0.11	+0.21 ± 0.17	+0.05
8	-0.01 ± 0.08	-0.03	-0.27 ± 0.10	-0.15	-0.25 ± 0.10	-0.14	+0.23 ± 0.12	+0.13
10	-0.02 ± 0.08	-0.08	-0.18 ± 0.10	-0.23	-0.18 ± 0.10	-0.19	+0.15 ± 0.11	+0.17
12	-0.03 ± 0.08	-0.23	-0.16 ± 0.10	-0.36	-0.13 ± 0.11	-0.29	+0.09 ± 0.10	+0.21
14	-0.03 ± 0.10	-0.41	-0.15 ± 0.18	-0.60	-0.03 ± 0.15	-0.11	+0.04 ± 0.12	+0.15

Table II. Conversion Probabilities for L_c = 2.50 m. in the FNAL 15-ft Chamber with TST

Conversion Probability	Percentage Neon Concentration (molar) 0	10	20	30	40	50	60	70	80	90	100
$P(1\gamma)$	.182	.465	.666	.802	.890	.943	.973	.989	.996	.998	.999
$P(2\gamma)$	.033	.216	.444	.644	.793	.890	.947	.978	.992	.997	.999
$P(3\gamma)$	.006	.100	.296	.516	.706	.840	.922	.967	.988	.996	.999
$P(4\gamma)$	.001	.047	.197	.415	.628	.792	.897	.957	.984	.995	.998
$P(5\gamma)$	--	.022	.131	.333	.559	.747	.873	.946	.980	.993	.998
$P(6\gamma)$	--	.010	.087	.267	.498	.705	.850	.936	.976	.992	.998
$P(7\gamma)$	--	.005	.058	.214	.443	.665	.827	.925	.972	.990	.997
$P(8\gamma)$	--	.002	.038	.172	.395	.628	.805	.915	.968	.889	.996
$P[1\gamma(1\pi^o)]$	.297	.498	.445	.317	.196	.108	.053	.022	.008	.003	.001
$P[3\gamma(2\pi^o)]$	.020	.215	.395	.409	.310	.191	.100	.043	.016	.005	.002
$P[5\gamma(3\pi^o)]$	.001	.070	.263	.395	.369	.255	.138	.062	.023	.008	.002
$P[7\gamma(4\pi^o)]$	--	.020	.156	.339	.391	.303	.179	.081	.031	.010	.003
$P[\geq 1\gamma(1\pi^o)]$	.330	.714	.889	.962	.989	.998	.999	.999	.999	.999	.999
$P[\geq 3\gamma(2\pi^o)]$	.020	.262	.642	.824	.938	.983	.997	.999	.999	.999	.999
$P[\geq 5\gamma(3\pi^o)]$	.009	.080	.350	.662	.867	.960	.988	.998	.999	.999	.999
$P[\geq 7\gamma(4\pi^o)]$	--	.022	.193	.511	.786	.931	.984	.996	.999	.999	.999

Table III. Comparison of Conversion Efficiencies for L_c = 170, 200, and 250 cm for 20% and 30% (atomic) neon concentrations

Conversion Probability	20% (atomic)[33% (molar)] Neon Concentration			30% (atomic)[45% (molar)] Neon Concentration		
	L_c = 170 cm	L_c = 200 cm	L_c = 250 cm	L_c = 170 cm	L_c = 200 cm	L_c = 250 cm
P(1 γ)	.698	.756	.833	.827	.873	.917
P(2 γ)	.488	.571	.694	.685	.763	.842
P(3 γ)	.340	.432	.578	.567	.666	.773
P(4 γ)	.237	.326	.481	.469	.582	.710
P(5 γ)	.166	.247	.401	.388	.508	.653
P(6 γ)	.116	.186	.334	.321	.444	.602
P(7 γ)	.081	.141	.279	.266	.388	.554
P(8 γ)	.057	.106	.232	.220	.340	.512
P [1 γ (1π^o)]	.422	.369	.278	.286	.222	.152
P [3 γ (2π^o)]	.412	.421	.322	.392	.339	.251
P [5 γ (3π^o)]	.301	.361	.402	.403	.387	.312
P [7 γ (4π^o)]	.195	.275	.372	.368	.394	.347
P [$\geq$ 1 γ (1π^o)]	.910	.939	.972	.971	.984	.994
P [$\geq$ 3 γ (2π^o)]	.649	.783	.867	.861	.921	.960
P [$\geq$ 5 γ (3π^o)]	.417	.547	.736	.724	.831	.913
P [$\geq$ 7 γ (4π^o)]	.252	.381	.604	.588	.394	.859

Table IV. Neutral Pion Topological Cross Sections and Event Production in a 4 event/μb exposure Expected for 200 GeV/c π^-p Interactions

π^0 Multiplicity	Estimated Topological Cross Section	Event
1	2.61 mb	10,440
2	3.62	14,480
3	3.92	15,680
4	3.73	14,920
5	2.80	11,200
6	1.74	6,900
7	0.91	3,640
8	0.42	1,680
9	0.20	800
10	0.07	280
11	0.03	120
12	0.007	30

Figure Captions

Fig. 1 Distribution of the invariant structure function $\pi^{-1} d\sigma/dy$ as a function of c.m. rapidity y for (a) final state π^- and (b) final state π^+ in 205 GeV/c $\pi^- p$ interactions. Distributions for lower energy data are shown for comparison. (Data from ref. 2.)

Fig. 2 Comparison of the inclusive γ distributions for 18.5 GeV/c $\pi^{\pm} p$ interactions (histogram) with Monte Carlo distributions assuming that the π^0 distribution was identical to that of the π^+ (dash-dot curve) or that of the π^- (dashed curve) produced in the same reactions. Distributions for the Feynman x variable and the square of the transverse momentum k_T^2 are shown for the $\pi^- p$ data in (a) and (b) respectively, and for the $\pi^+ p$ data in (c) and (d) respectively. (Data from ref. 4.)

Fig. 3 Plots showing the approach to scaling of (a) the structure function for the central region, $-0.02 \leq x \leq 0.02$, and (b) the integral of the structure function $G(p_\ell) = \int (E/\sigma_T)(d^2\sigma dp_\ell \, dp_T^2) dp_T^2$ for $p_\ell < 0$, the target fragmentation region, for various $\pi^{\pm} p$ inclusive reactions. (Data from ref. 2.)

Fig. 4 Distributions of $\pi^{-2} d\sigma/dy_1 dy_2$ as a function of y_2 for various ranges of y_1 in the two-particle reactions at 205 GeV/c: (a) $\pi^- p \to \pi^{ch} + \pi^{ch} + \ldots$; (b) $\pi^- p \to \pi^- + \pi^- + \ldots$; (c) $\pi^- p \to \pi^+ + \pi^+ + \ldots$; (d) $\pi^- p \to \pi^- + \pi^+ + \ldots$. Various ranges of y_1 are indicated by different symbols as shown on

the figure. (Data from ref. 2.)

Fig. 5 Contour plots showing lines of constant $R(y_1, y_2)$ as a function of y_1 and y_2 for the two-particle inclusive reactions at 205 GeV/c: (a) $\pi^- p \rightarrow \pi^{ch} + \pi^{ch} + \ldots$; (b) $\pi^- p \rightarrow \pi^- + \pi^- + \ldots$; (c) $\pi^- p \rightarrow \pi^+ + \pi^+ + \ldots$; (d) $\pi^- p \rightarrow \pi^- + \pi^+ + \ldots$. (Data from ref. 2.)

Fig. 6 Event types bearing on the definition of clusters. (From Quigg and Chao, ref. 15)

Fig. 7 Radiation length and interaction length for 200 GeV/c π^- as a function of neon concentration in the neon/hydrogen mixture.

Fig. 8 Gamma conversion probabilities for a nominal 2.50 meter conversion path as a function of neon concentration in the neon/hydrogen mixture.

Fig. 9 Multiple scattering error for minimum-ionizing tracks in a 20 k gauss magnetic field as a function of track length and neon concentration.

Fig. 10 Projection of the liquid phase separation boundary on the temperature-Neon concentration plane (data from Streett and Jones, ref. 18).

Fig. 11 Temperature and pressure differences between target liquid and chamber liquid for the condition of constant bubble density for tracks in the TST and chamber. Solid curves refer to hydrogen-filled TST, dashed curves to a deuterium-filled TST in a neon/hydrogen mixture. (Similar curves could be drawn for the condition of constant bubble growth rate for tracks in the TST and chamber, using the data of Horlitz, Wolf, and Horigel, ref. 19.)

Fig. 12 Angular distribution (LAB) of π^+ mesons produced in 205 GeV/c π^-p interactions. It is assumed that the angular distribution of the π^o will be similar to that of the π^+.

Fig. 13 Overall drawing of the TST configuration to be provided for the 15-ft FNAL chamber.

Fig. 14 Schematic of the fill-and-vent servo system for the TST to be provided for the 15-ft FNAL chamber.

Fig. 15 July, 1974 engineering run with a 57 in. x 21-3/4 in. x 4-1/4 in. plexiglass TST in the Brookhaven 80-in. bubble chamber. The cooling loop, fill/vent valve, vapor pressure bulb, and strain gauge (bottom edge center) are evident. The chamber was filled with ~77 mole % neon. The operating conditions at the time of the photograph were T (chamber) = 29.6° K, T (target) = 28.7° K, p_0 = 126 psia, p_{min} = 75 psia under which conditions the chamber, but not the target, was track-sensitive.

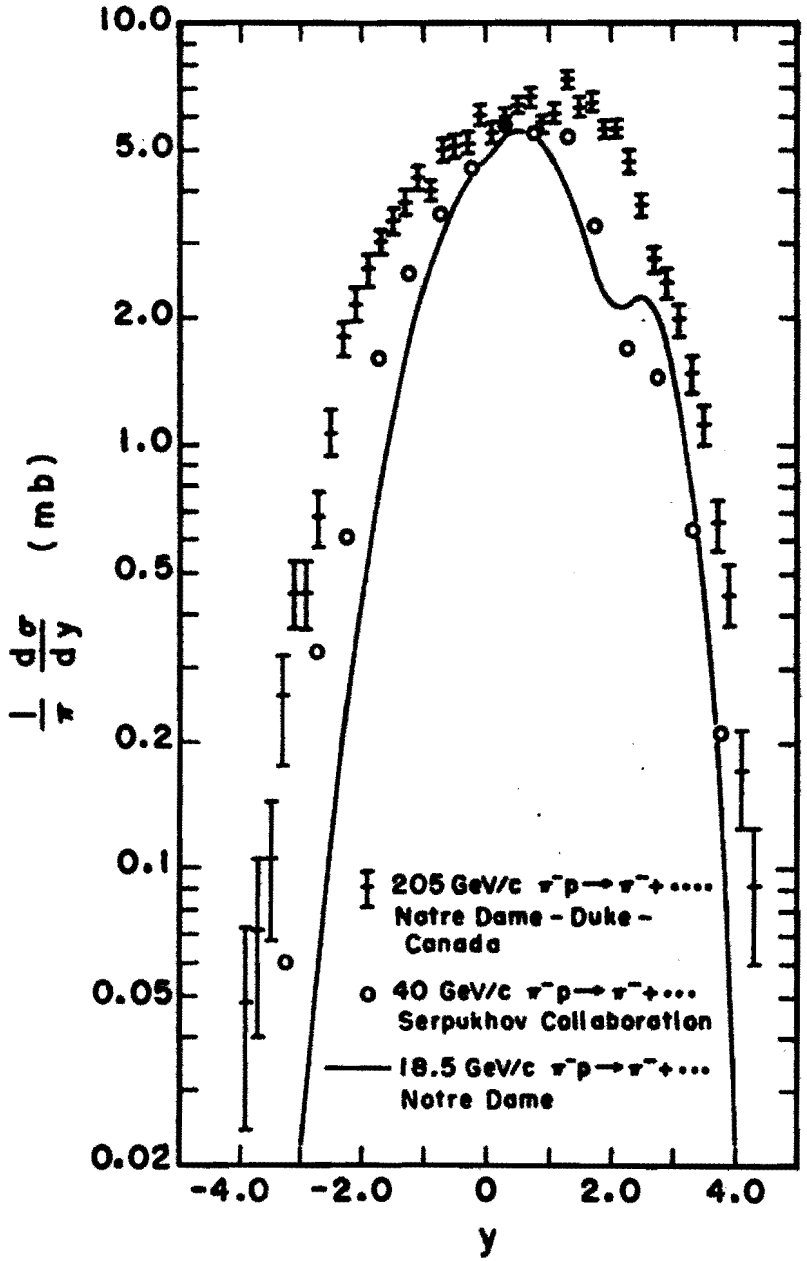
10.0
5.0
2.0
1.0
0.5
0.2
0.1
0.05
0.02
-4.0
-2.0
0
2.0
4.0
y
$\frac{1}{\sigma}\frac{d\sigma}{dy}$ (mb)
205 GeV/c $\pi^- p \to \pi^- + \cdots$
Notre Dame - Duke - Canada
40 GeV/c $\pi^- p \to \pi^- + \cdots$
Serpukhov Collaboration
18.5 GeV/c $\pi^- p \to \pi^- + \cdots$
Notre Dame

Fig. 1a

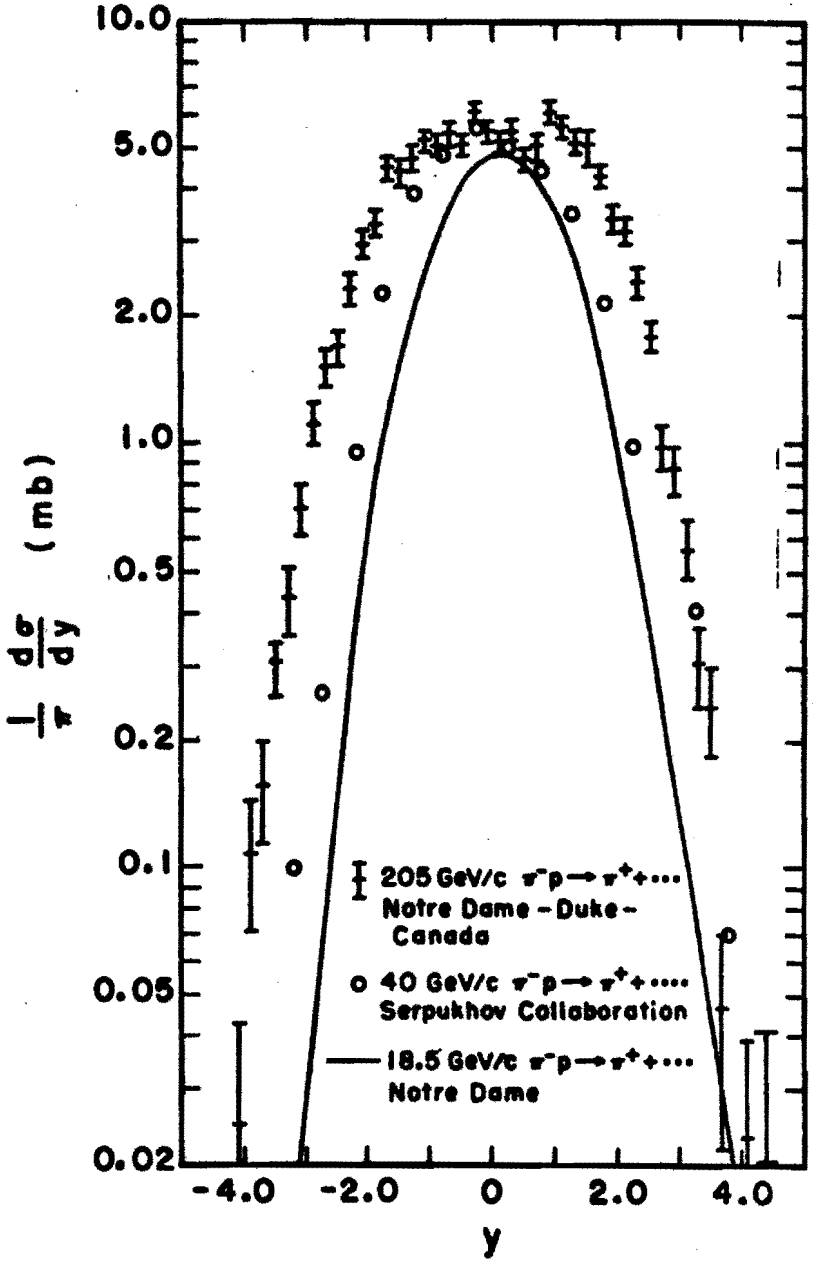
10.0
5.0
2.0
1.0
0.5
0.2
0.1
0.05
0.02
-4.0
-2.0
0
2.0
4.0
y
$\frac{1}{\sigma}\frac{d\sigma}{dy}$ (mb)
205 GeV/c $\pi^- p \to \pi^+ + \cdots$
Notre Dame - Duke - Canada
40 GeV/c $\pi^- p \to \pi^+ + \cdots$
Serpukhov Collaboration
18.5 GeV/c $\pi^- p \to \pi^+ + \cdots$
Notre Dame

Fig. 1b

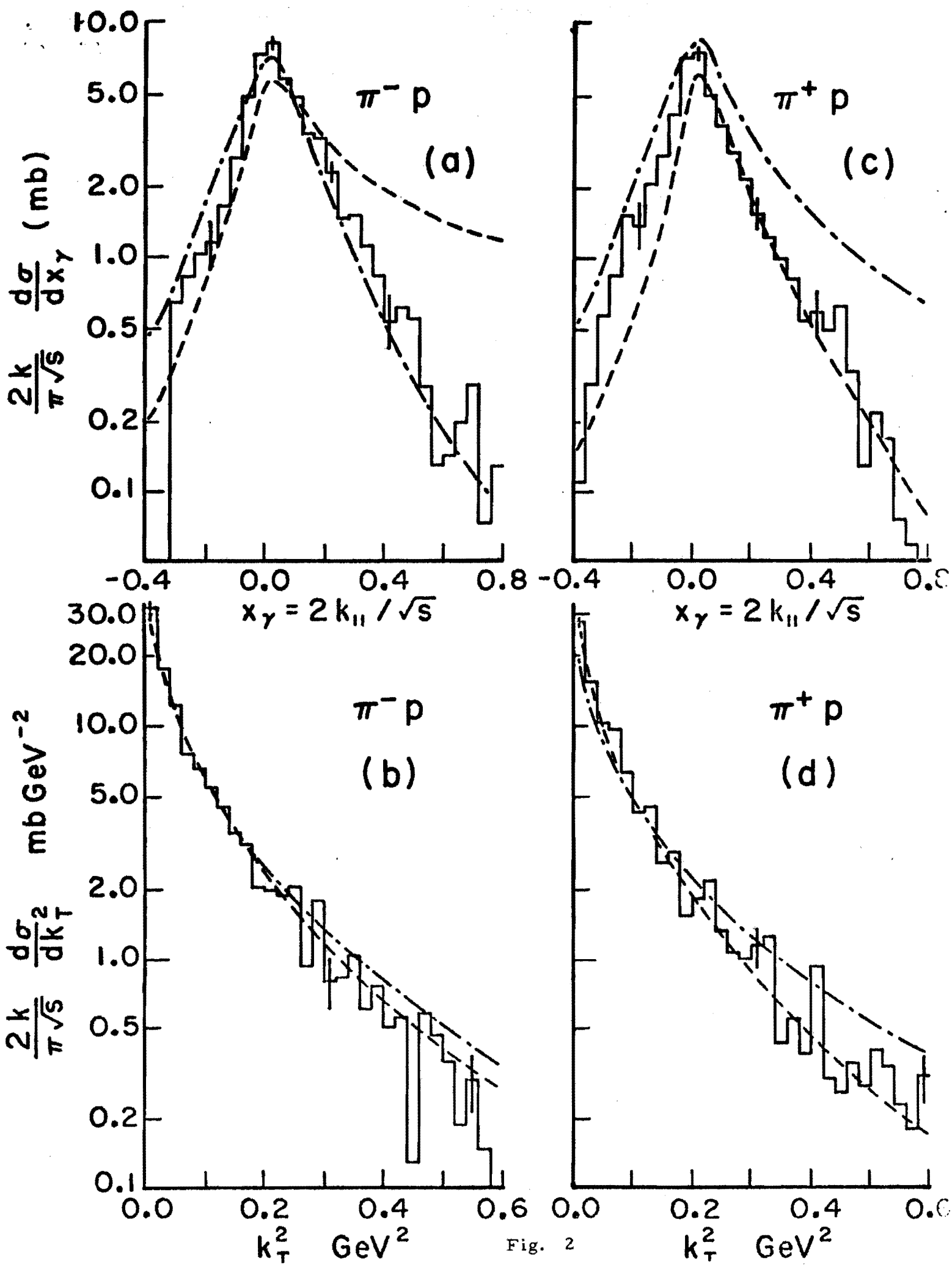
π⁻ p
(a)
π⁺ p
(c)
$\frac{2k}{\pi\sqrt{s}} \frac{d\sigma}{dx_\gamma}$ (mb)
$x_\gamma = 2k_{\parallel} / \sqrt{s}$
π⁻ p
(b)
π⁺ p
(d)
$\frac{2k}{\pi\sqrt{s}} \frac{d\sigma}{dk_T^2}$ mb GeV^{-2}
k_T^2 GeV^2

Fig. 2

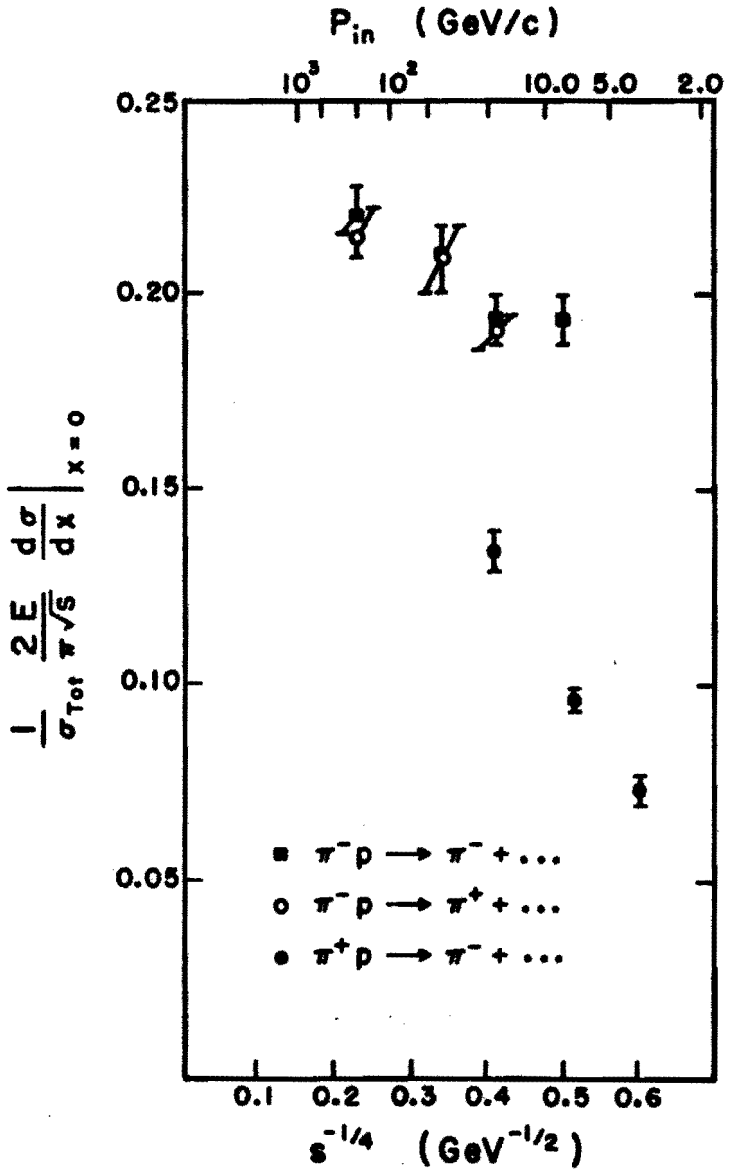
P_in (GeV/c)
10^3
10^2
10.0
5.0
2.0
0.25
0.20
0.15
0.10
0.05
1/σ_Tot π√S 2E dσ/dx |x=0
■ π⁻p → π⁻ + ...
○ π⁻p → π⁺ + ...
● π⁺p → π⁻ + ...
0.1
0.2
0.3
0.4
0.5
0.6
s^-1/4 (GeV^-1/2)

Fig. 3a

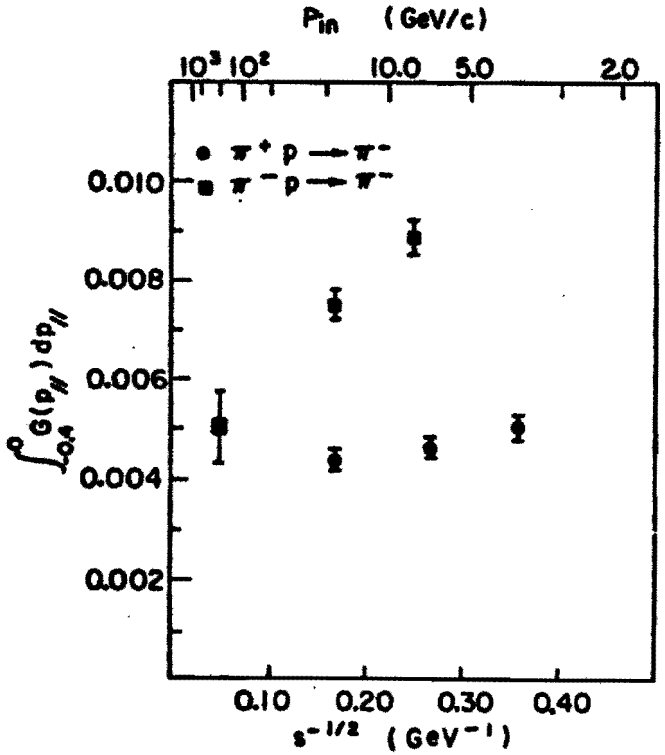
P_in (GeV/c)
10^3
10^2
10.0
5.0
2.0
● π⁺p → π⁻
■ π⁻p → π⁻
0.010
0.008
0.006
0.004
0.002
∫ G(p_//) dp_//
0.10
0.20
0.30
0.40
s^-1/2 (GeV^-1)

Fig. 3b

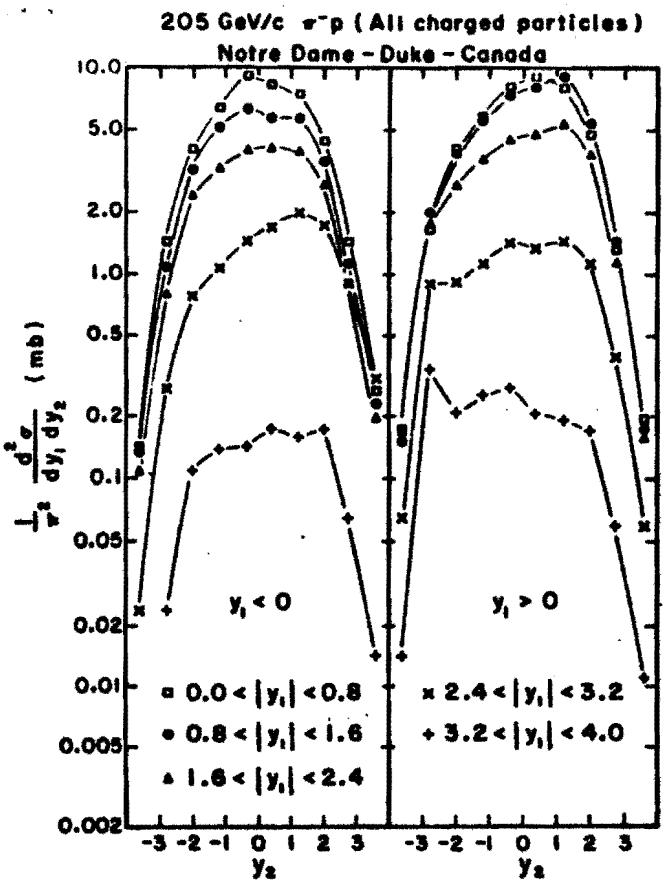

Fig. 4a

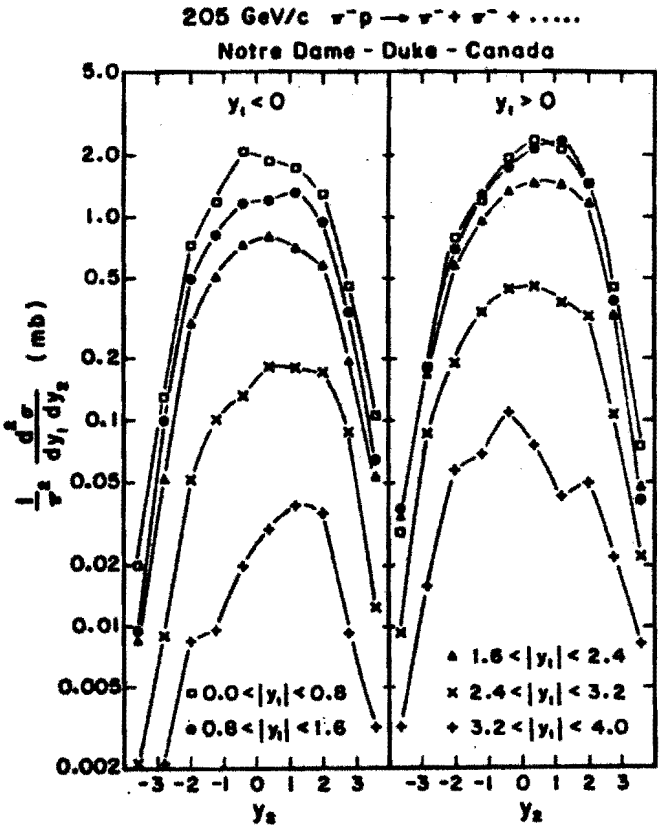

Fig. 4b

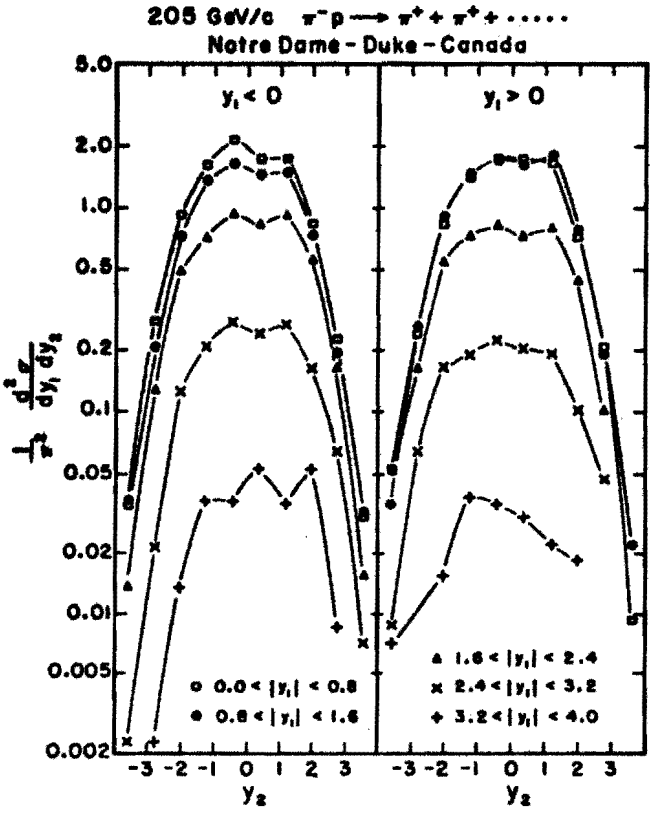

Fig. 4c

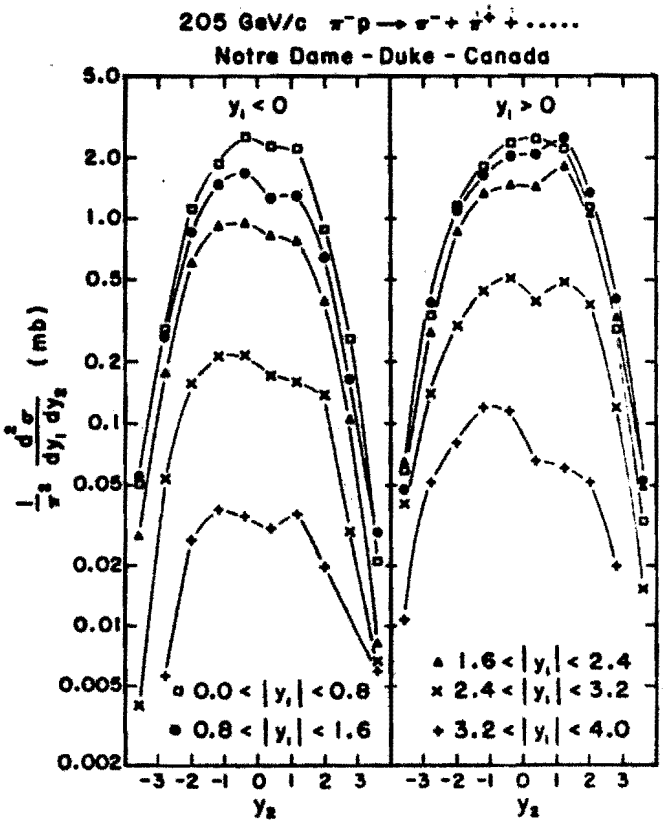

Fig. 4d

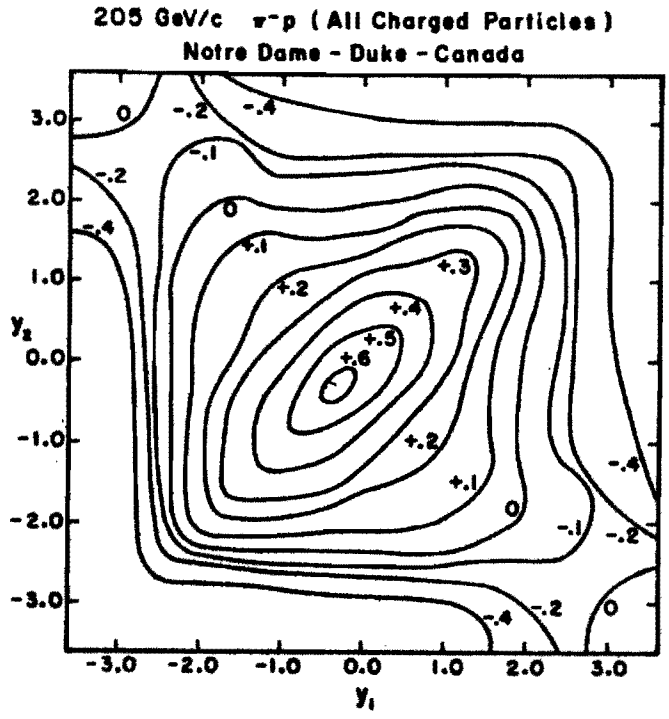

Fig. 5a

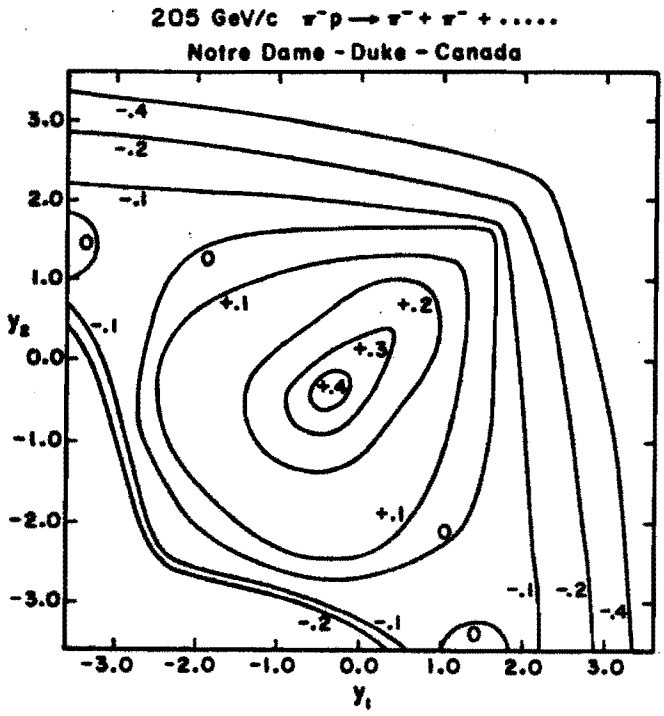

Fig. 5b

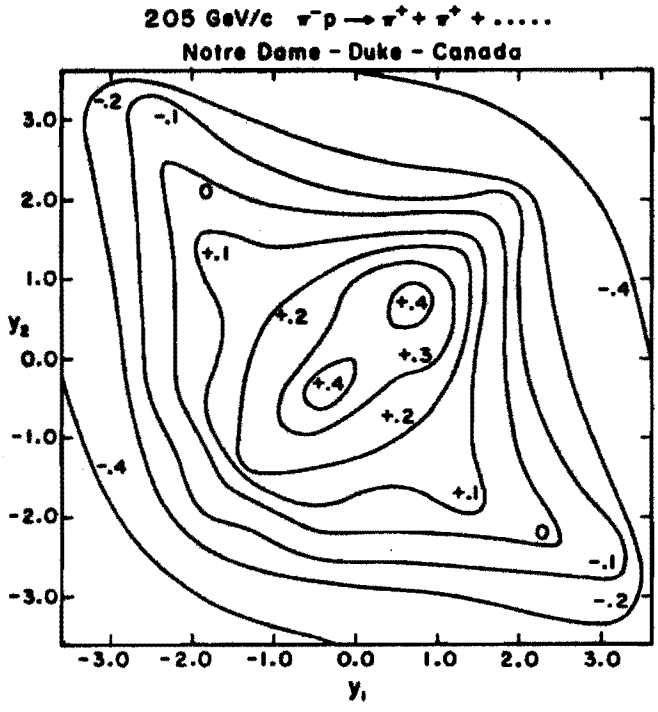

Fig. 5c

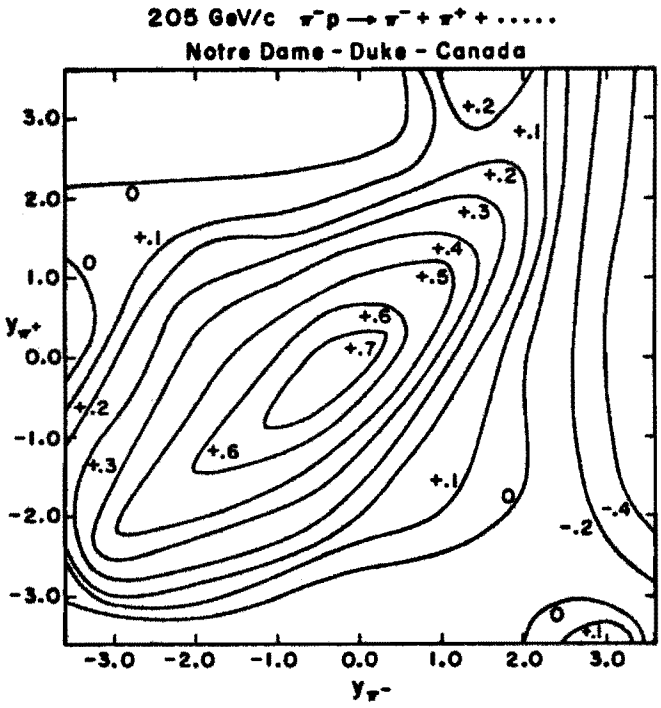

Fig. 5d

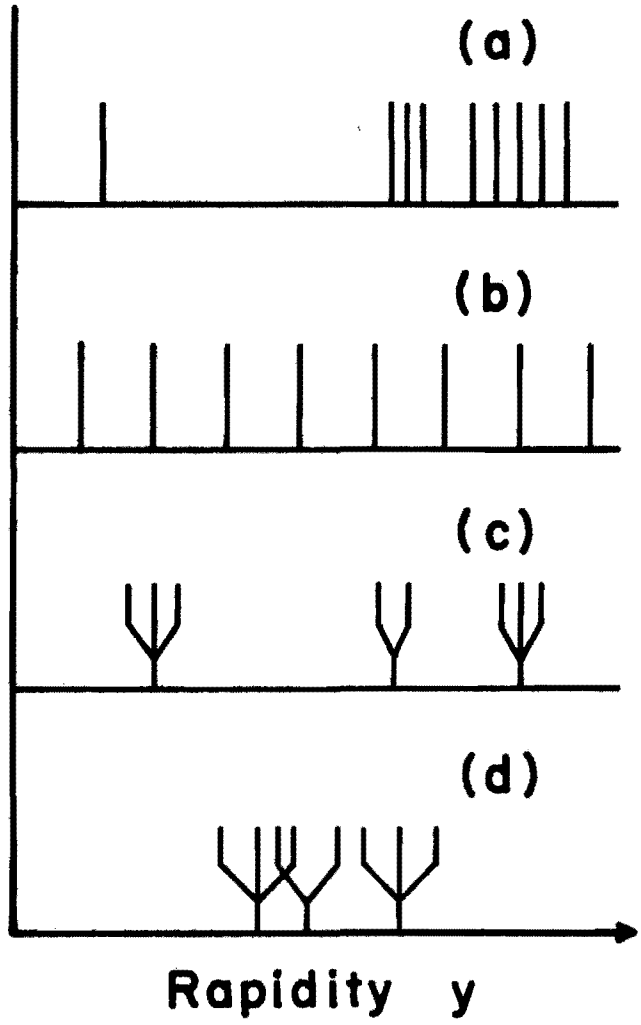

Fig. 6

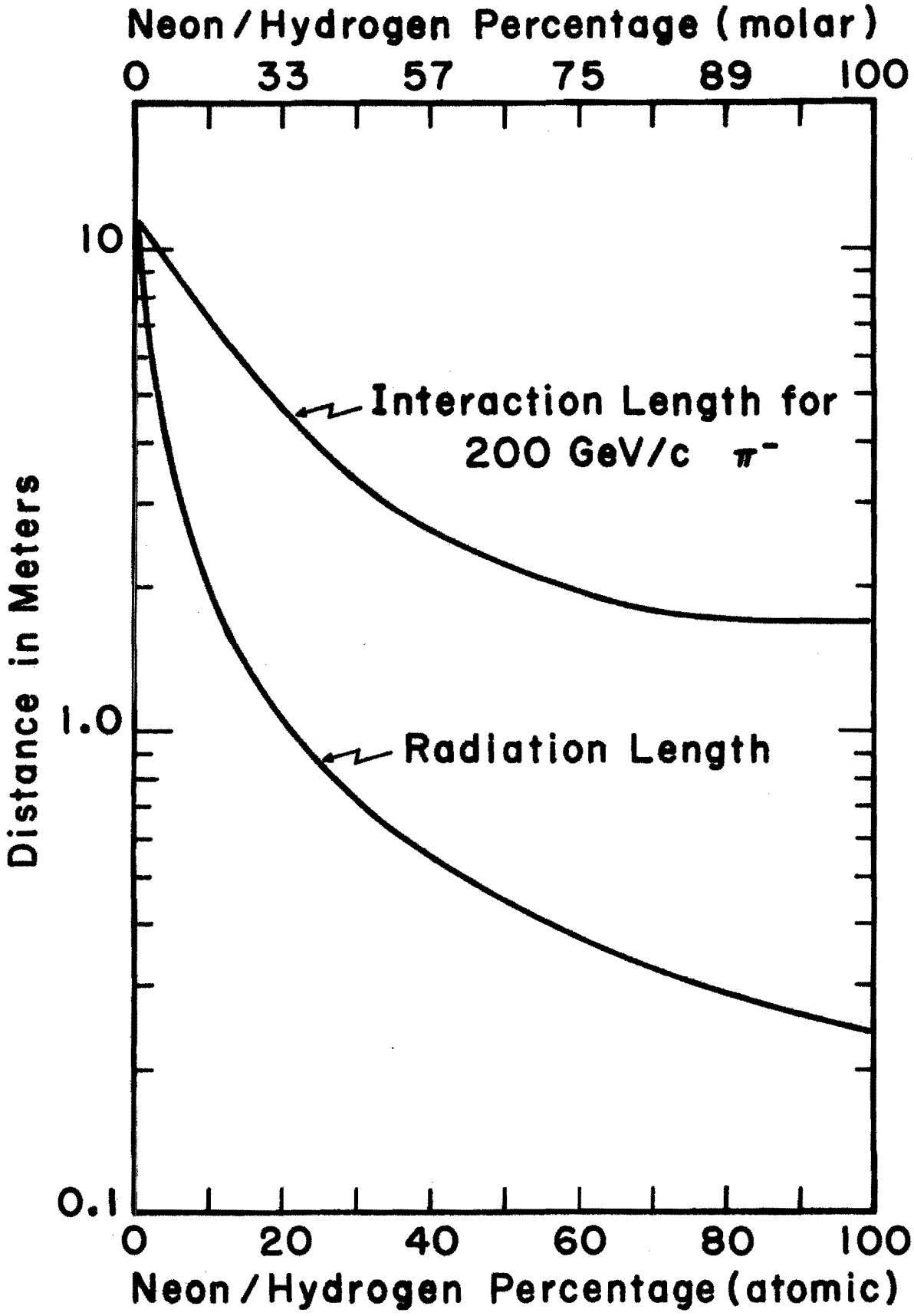
Neon / Hydrogen Percentage (molar)
0
33
57
75
89
100
10
1.0
0.1
Distance in Meters
Interaction Length for
200 GeV/c π⁻
Radiation Length
0
20
40
60
80
100
Neon / Hydrogen Percentage (atomic)

Fig. 7

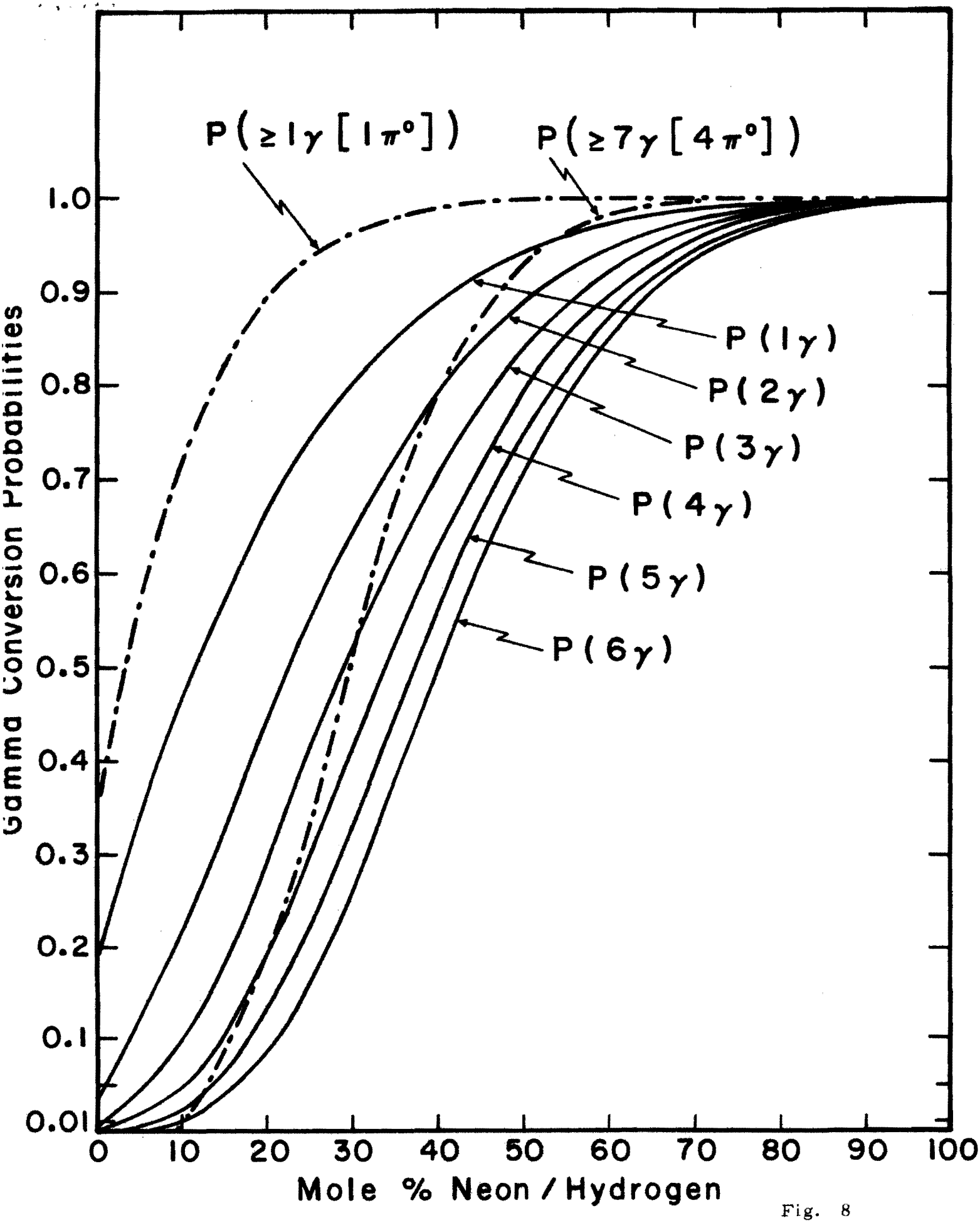
P(≥1γ [1π°])
P(≥7γ [4π°])
P(1γ)
P(2γ)
P(3γ)
P(4γ)
P(5γ)
P(6γ)
Gamma Conversion Probabilities
1.0
0.9
0.8
0.7
0.6
0.5
0.4
0.3
0.2
0.1
0.01
0
10
20
30
40
50
60
70
80
90
100
Mole % Neon / Hydrogen

Fig. 8

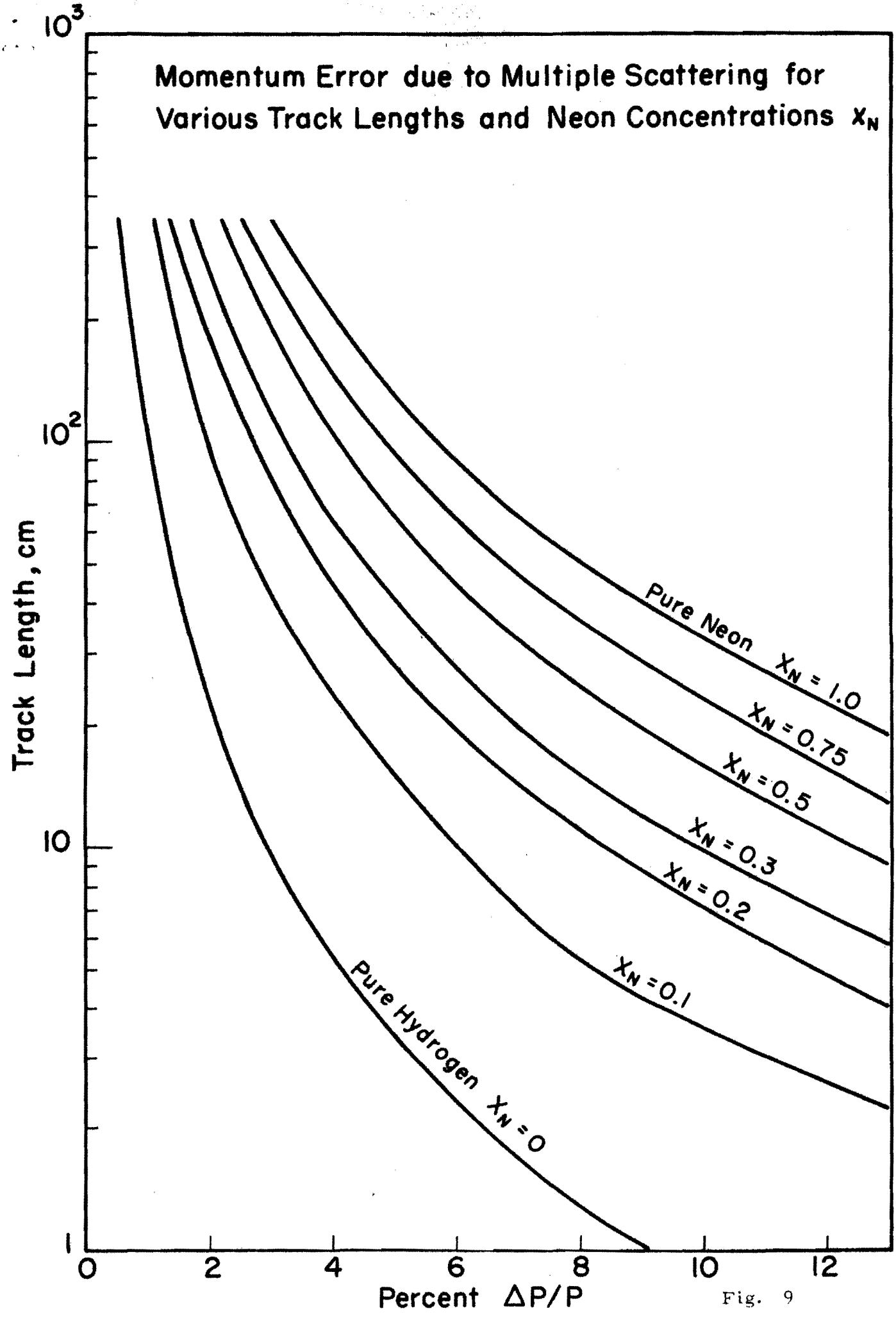
Momentum Error due to Multiple Scattering for
Various Track Lengths and Neon Concentrations X_N
Track Length, cm
10^3
10^2
10
1
0
2
4
6
8
10
12
Percent ΔP/P
Pure Neon $X_N = 1.0$
$X_N = 0.75$
$X_N = 0.5$
$X_N = 0.3$
$X_N = 0.2$
$X_N = 0.1$
Pure Hydrogen $X_N = 0$

Fig. 9

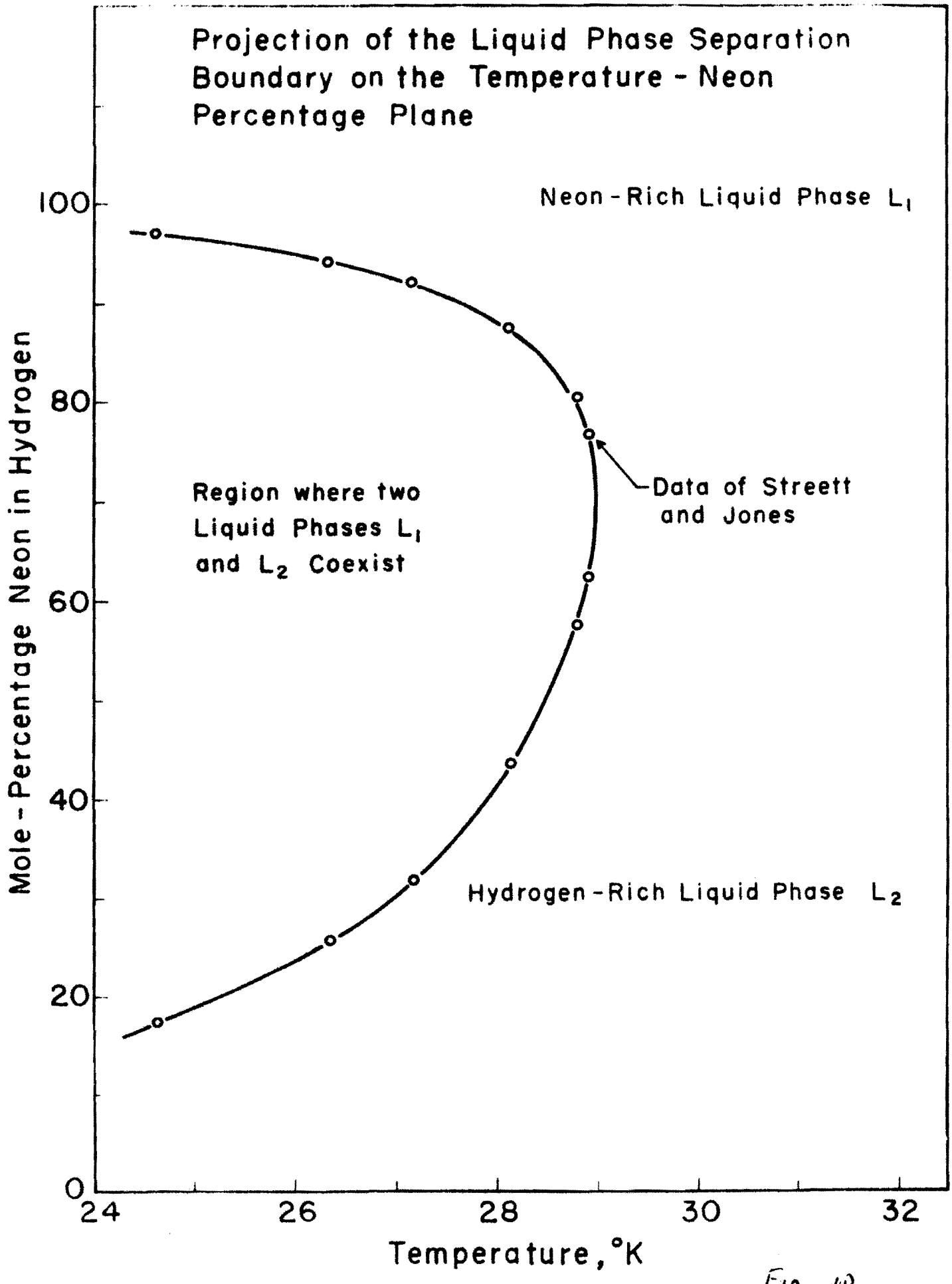
Projection of the Liquid Phase Separation Boundary on the Temperature - Neon Percentage Plane
Neon-Rich Liquid Phase L_1
Region where two Liquid Phases L_1 and L_2 Coexist
Data of Streett and Jones
Hydrogen-Rich Liquid Phase L_2
Mole-Percentage Neon in Hydrogen
100
80
60
40
20
0
24
26
28
30
32
Temperature, °K

Fig. 10

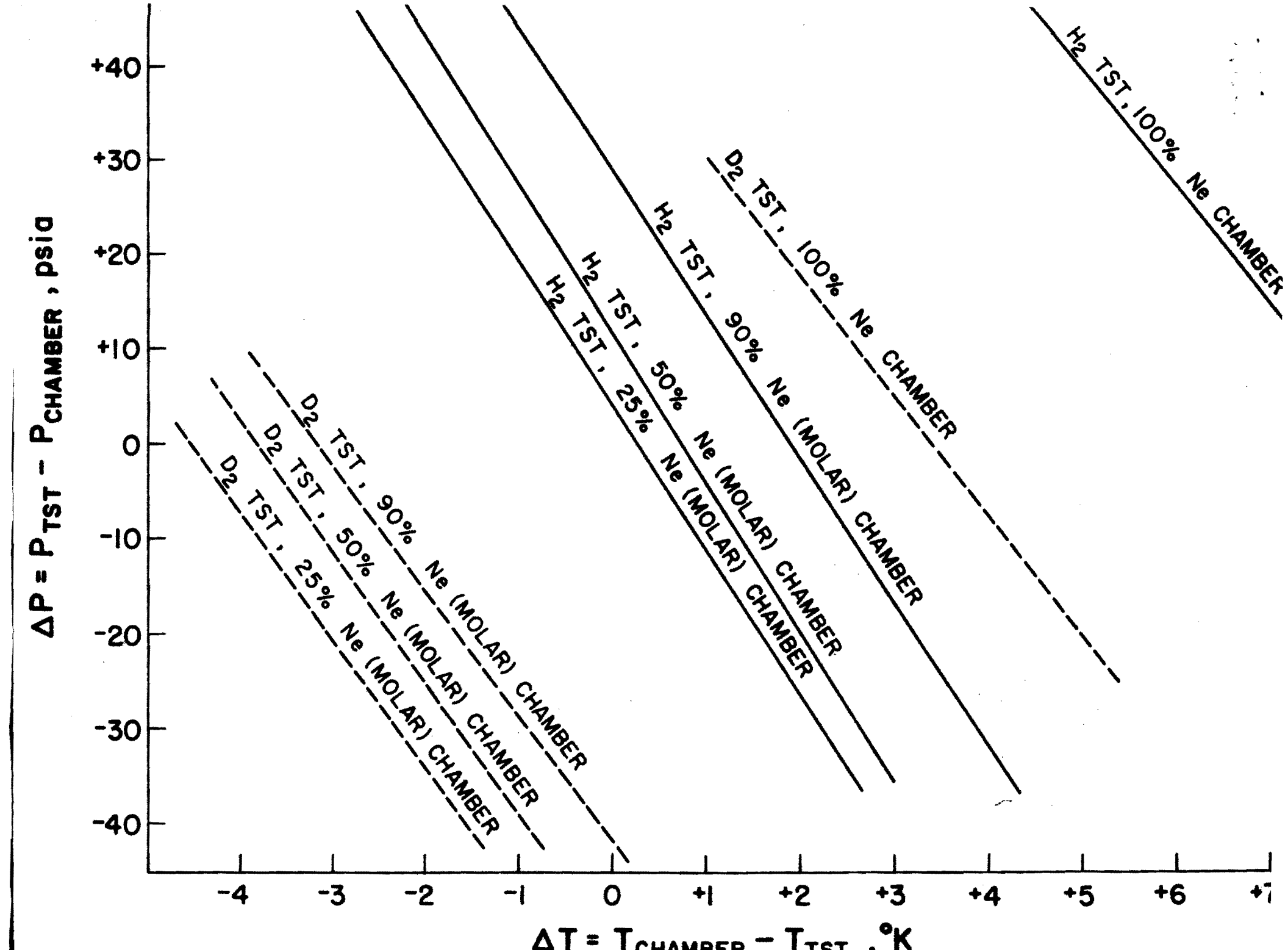
+40
+30
+20
+10
0
-10
-20
-30
-40
ΔP = P_TST - P_CHAMBER , psia
-4
-3
-2
-1
0
+1
+2
+3
+4
+5
+6
+7
ΔT = T_CHAMBER - T_TST , °K
H2 TST, 100% Ne CHAMBER
H2 TST, 90% Ne (MOLAR) CHAMBER
H2 TST, 50% Ne (MOLAR) CHAMBER
H2 TST, 25% Ne (MOLAR) CHAMBER
D2 TST, 100% Ne CHAMBER
D2 TST, 90% Ne (MOLAR) CHAMBER
D2 TST, 50% Ne (MOLAR) CHAMBER
D2 TST, 25% Ne (MOLAR) CHAMBER

Fig. 11

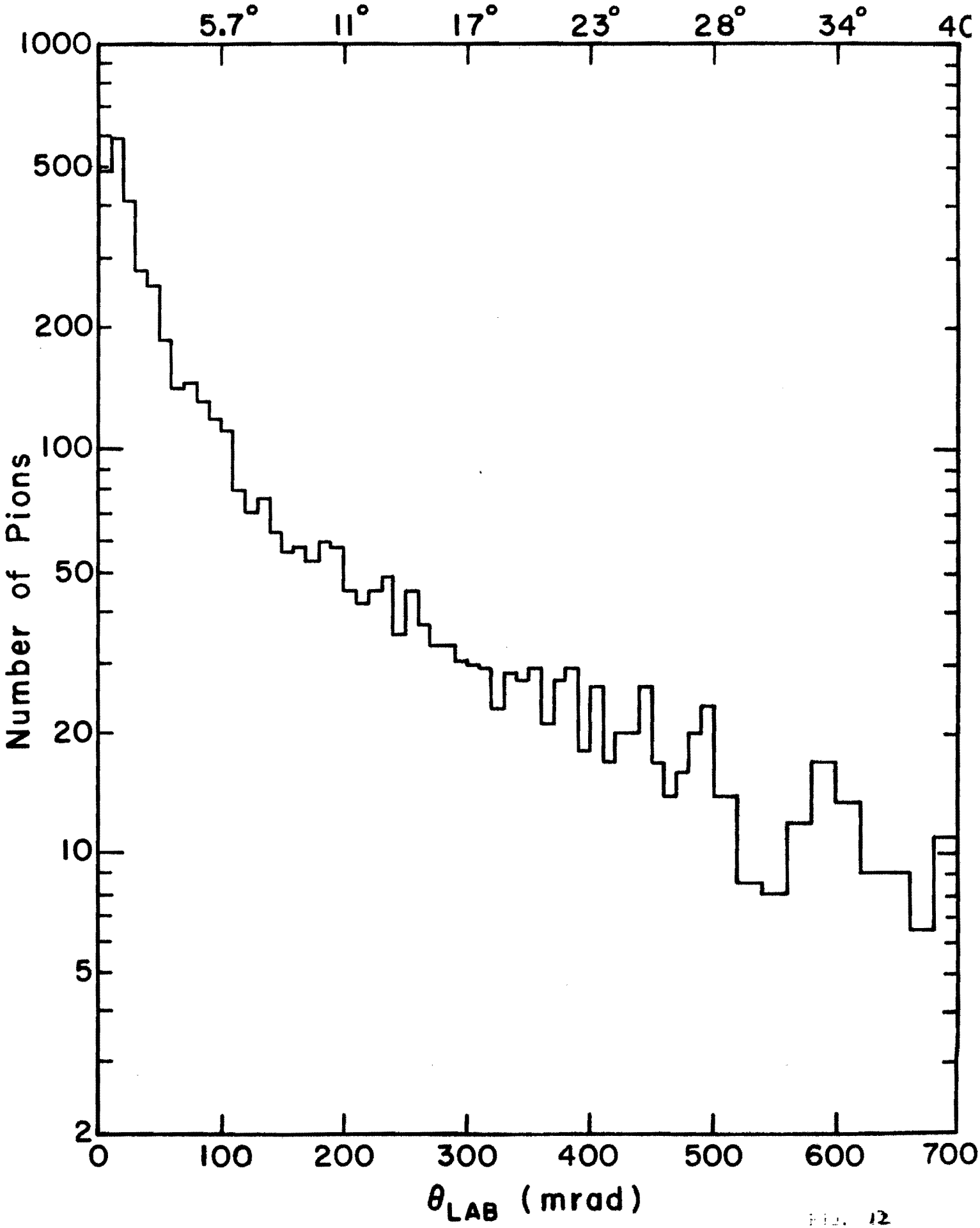
5.7°
11°
17°
23°
28°
34°
40
1000
500
200
100
50
20
10
5
2
Number of Pions
0
100
200
300
400
500
600
700
θLAB (mrad)

FIG. 12

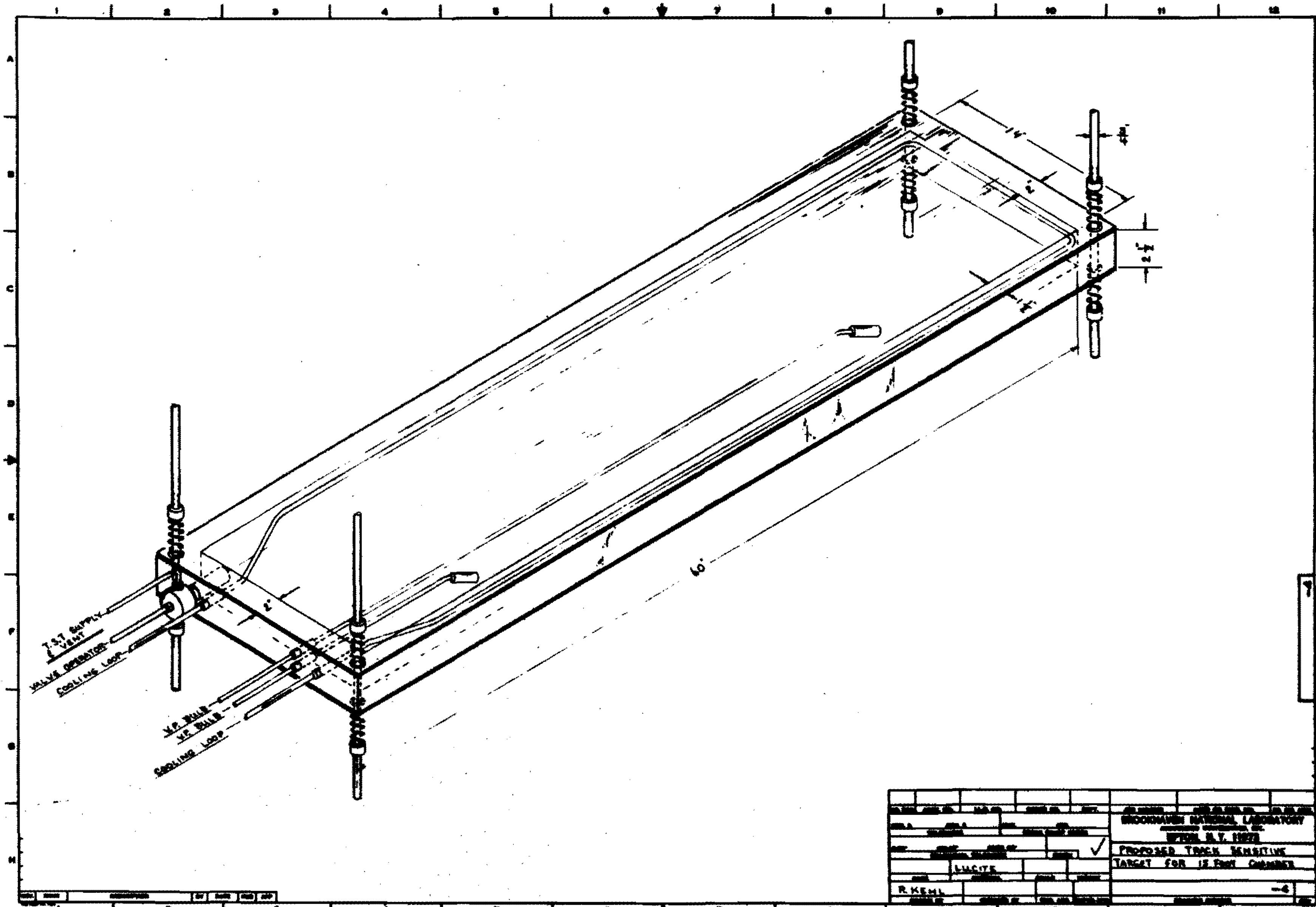
T.S.T SUPPLY & VENT
VALVE OPERATOR
COOLING LOOP
V.P. BULB
V.P. BULB
COOLING LOOP
60"
14"
PROPOSED TRACK SENSITIVE
TARGET FOR 15 FOOT CHAMBER
LUCITE
R. KEHL

Fig. 13

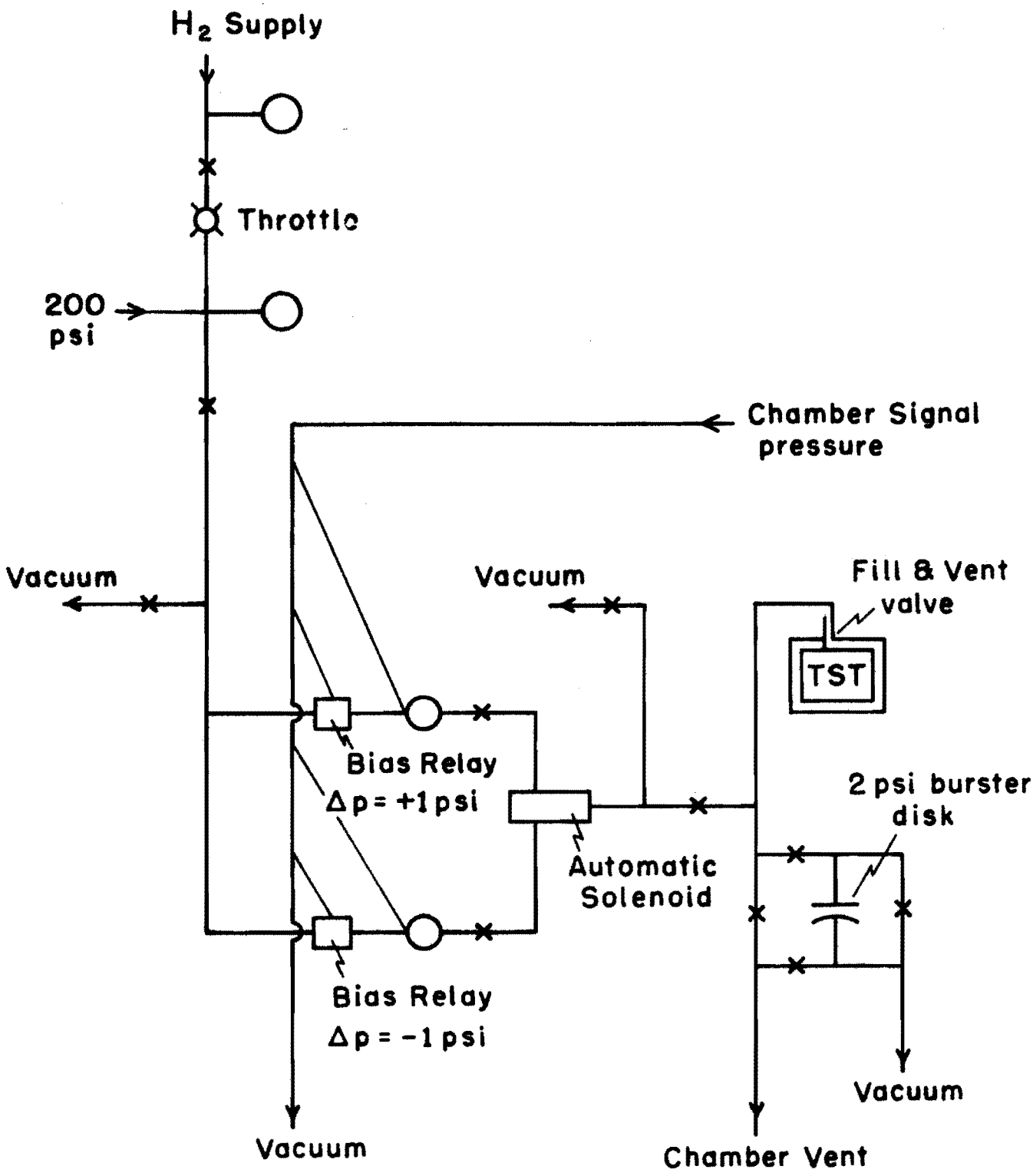
H_2 Supply
Throttle
200 psi
Chamber Signal pressure
Vacuum
Vacuum
Fill & Vent valve
TST
Bias Relay
Δp = +1 psi
2 psi burster disk
Automatic Solenoid
Bias Relay
Δp = −1 psi
Vacuum
Vacuum
Chamber Vent

Fig. 14

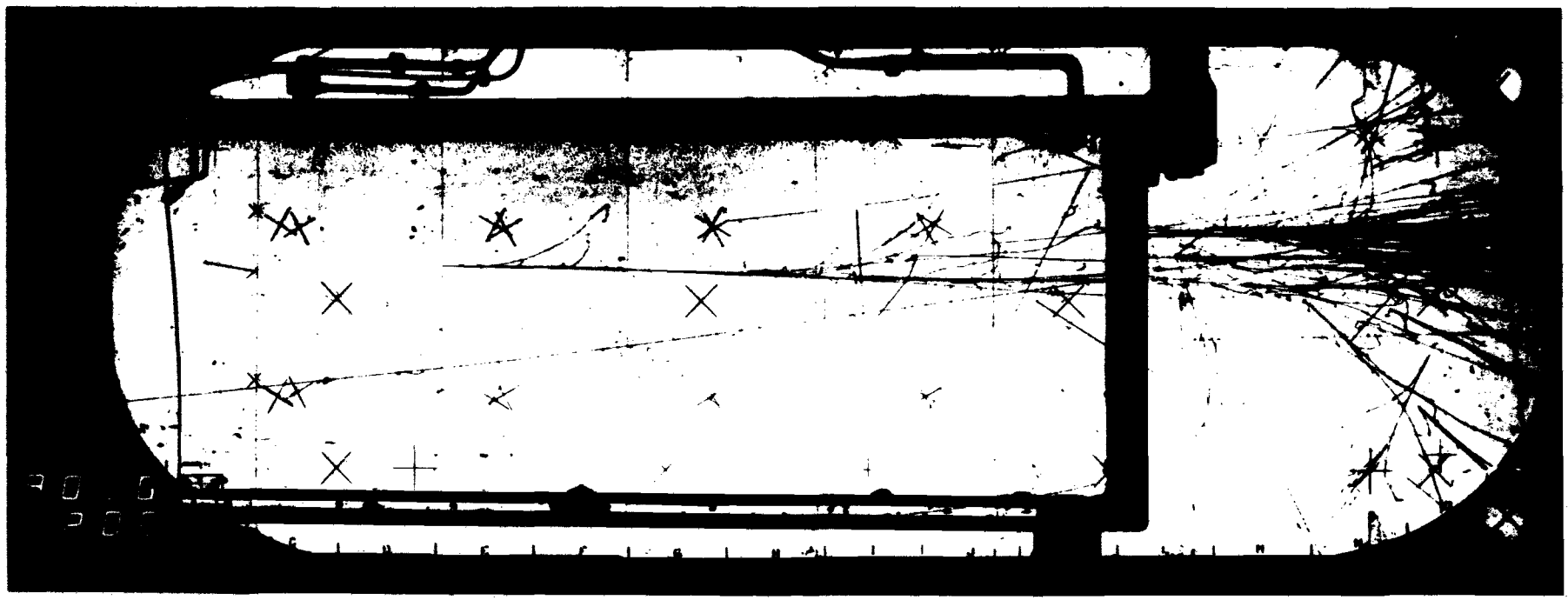

Fig. 15